DOI 10.5162/EUROSENSORSXXXVI/OT6.79

Development and Characterization of Microfluidic Channels for Chromatography-on-a-Chip Applications

Rodolfo G. Rodrigues[1], Rafael Batista[1], Ana M. Azevedo[2,3], Virginia Chu[1], João Pedro Conde[1,3],

[1] Instituto de Engenharia de Sistemas e Computadores–Microsistemas e Nanotecnologias (INESC MN), Rua Alves Redol, 1000-029 Lisbon, Portugal,
[2] IBB—Institute for Bioengineering and Biosciences, Instituto Superior Técnico, Universidade de Lisboa, 1049-001 Lisboa, Portugal,
[3] Department of Bioengineering, Instituto Superior Técnico, Avenida Rovisco Pais, 1049-001 Lisbon, Portugal

Corresponding Author's e-mail address: joao.conde@tecnico.ulisboa.pt

Summary:

In this work, we designed and fabricated a microfluidic device to perform chromatographic separations. The device consists of a column filled with silica microbeads between smaller height channels working as a frit. To characterize the column efficiency, the breakthrough method was used with a solution of fluorescein isothiocyanate (FITC) in ethanol and by measuring the fluorescence signal. Several mobile phase velocities were tested to obtain retention times and plate heights.

Keywords: Microfluidics, Liquid Chromatography, Cyclic Olefin Copolymer, Breakthrough Curves, Silica Microbeads

Background

Liquid chromatography is a separation technique widely used for the detection of molecules present in complex solutions [1], but it requires trained users in a laboratory and consumes a large quantity of reagents. On the other hand, microfluidics is a technology that has the potential to significantly improve biological and chemical analysis by being inexpensive, portable, and fast [2]. The miniaturization of liquid chromatography using microfluidics combines both technologies but has not been studied in detail. This work aims to develop microfluidic channels for liquid chromatography that can have separation performances comparable to those obtained at macroscale.

Methodology

Computer numerical control (CNC) milling was used directly in cyclic olefin copolymer (COC) plates with a flat endmill with 0.4 mm diameter. The feed rate was maintained at 100 mm/min at 12000 rpm. The device sealing and connections are described elsewhere [2]. Briefly, the machined COC is drilled and sealed against the same type of COC by thermal bonding. After the sealing, PEEK connectors are glued to the device. Silica (SiO_2) microbeads with a diameter between 45 and 75 µm diluted in PEG 8000 30% (w/w) are loaded into the device with the help of a syringe pump. The design used (see Fig. 1) consists of three 1 cm long channels with 100 µm height, and between them are 20 µm height channels to trap the microbeads inside the middle channel.

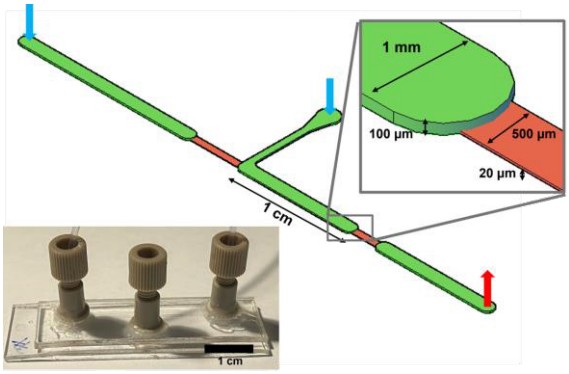

Fig. 1. Schematics of the chip design and a fabricated device in-use.

For breakthrough curve experiments, a solution of 12 µg/mL of fluorescein isothiocyanate (FITC) in ethanol was used, and the signal was acquired by fluorescence and quantified using ImageJ. The solution is flowed into the device at the desired flow, and time zero is taken when the fluorescence solution reaches the beginning of the microbeads. Several flow rates of the mobile phase were tested between 0.5 µL/min and 5 µL/min.

Results

In this device, we have a column of 1 cm in length packed with SiO_2 beads. A simple way to assess the column performance is by using the breakthrough curve method (or frontal chromatography). By performing breakthrough curves, we are observing the concentration of adsorbed analyte as a function of time, expecting the system to be fully saturated at the end of the experiment. In this case, our analyte was the fluorophore FITC, so the increasing adsorption was observed using a fluorescence microscope. In Fig. 2A are represented the breakthrough curves obtained for each flowrate tested (0.5 µL/min, 1 µL/min, 2.5 µL/min, and 5 µL/min).

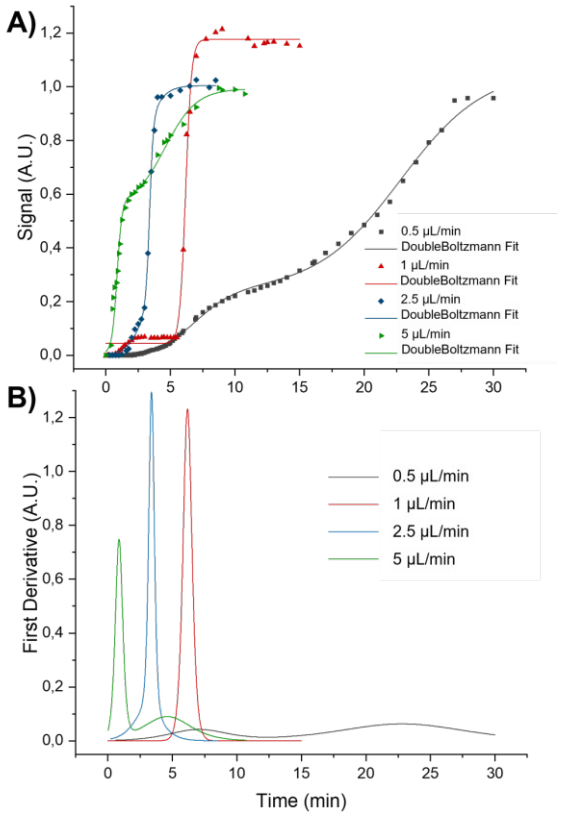

Fig. 2. A) Breakthrough curves and B) First Derivative plotted as a function of time for each flowrate.

To analyze the breakthrough data, the first derivative is calculated to obtain a pulse function, as seen in Fig. 1B. For all flowrates except for the 0.5 µL/min, a clear peak is observed, and as expected, the higher the flowrate, the closer to the origin is the peak. This system shows no retention of the FITC due to chemical interactions with SiO_2 beads, but the flow path is still interrupted by the beads, hence the retention times obtained. As for the 0.5 µL/min condition, the observed behavior may possibly be due to the B term of the van Deemter equation, the axial diffusion. Since the flow rate is lower, the residence time is longer, allowing the FITC to have more time to diffuse longitudinally and perhaps also within the pores. From the peak analysis it is possible to obtain the retention time (R_t) and the full width at half maximum (*FWHM*), and with these values to calculate the number of plates (N) and the plate height (H). At 1 µL/min we obtained 286 plates with a R_t of 6.17 min, resulting in a plate height of 34.99 µm. As expected, the retention time decreased for the other flow rates, being 3.37 min and 0.86 min for 2.5 µL/min and 5 µL/min, respectively, resulting in a decrease of the number of plates and increase of the plate height. For 2.5 µL/min we obtained 180 plates and H = 55.49 µm for 5 µL/min we obtained 9 plates and H = 1081.44 µm.

According to these results, using our microfluidic device we achieved the lowest plate height at 1 µL/min. By normalizing the number of plates, we obtained 28580 plates/m which is close to the range needed for HPLC [3].

Conclusions

Using our microfluidic device with a 1 cm long column and silica microbeads with a diameter between 45 and 75 µm we were able to achieve separation performances near the HPLC range. Increasing column length and decreasing microbead diameter to 5 µm is expected to drastically improve our separation efficiency, allowing us to obtain a device directly comparable to macroscale liquid chromatographic systems.

Acknowledgements

The authors thank the Fundação para a Ciência e a Tecnologia (FCT) for funding through the project VineSense (PTDC/BAA-DIG/4735/2020) [DOI: 10.54499/PTDC/BAA-DIG/4735/2020], the Research Unit INESC MN through the BASE (UIDB/0536/2020) [DOI: 10.54499/UIDB/05367/2020] and PROGRAMTICO (UIDP/0536/2020) [DOI: 10.54499/UIDP/05367/2020] programs, and doctoral grant for R. Rodrigues (2022.14483.BD).

References

[1] Y.I. Yashin, A.Y. Yashin, Chapter 10 – Liquid Chromatography, in *Chemical Analysis of Food: Techniques and Applications*, 285-310 (2012); doi: 10.1016/B978-0-12-384862-8.00010-8

[2] R.G. Rodrigues, P.G.M. Condelipes, R.R. Rosa, V. Chu, J.P. Conde, Scalable Processing of Cyclic Olefin Copolymer (COC) Microfluidic Biochips, *Micromachines* 14, 1837 (2023); doi: 10.3390/mi14101837

[3] S. Moldoveanu, V. David, Selection of the HPLC Method in Chemical Analysis (2017); ISBN: 978-0-12-803684-6

DOI 10.5162/EUROSENSORSXXXVI/OT6.80

Molecular weight measurement of cattle-emitted gases using whistle acoustic signals

Michitaka Yamamoto[1], *Rinka Yoshioka*[1], *Seiichi Takamatsu*[1], *Toshihiro Itoh*[1]
[1] *Department of Precision Engineering, Graduate School of Engineering, The University of Tokyo, 7-3-1 Hongo, Bunkyo-ku 113-8656, Tokyo, Japan*

Corresponding Author's e-mail address: yamamoto-michitaka@g.ecc.u-tokyo.ac.jp

Summary:
We experimentally revealed that the effect of temperature can theoretically be compensated in our proposed measurement method of the molecular weight of gas using whistles. The effect of temperature change on the molecular weight was around 0.03/°C, which is almost consistent with the theory. Furthermore, gas measurement with unknown molecular weight collected from cattle rumen fluid was demonstrated, with a molecular weight resolution of at least less than 1.5.

Keywords: sound and acoustic, gas sensor, molecular weight, Whistle, cattle

Introduction

There has been an increasing demand for simple measurement methods of gases; methane gas emitted by cattle has attracted much attention as a cause of global warming, and a simple method for measuring exhaled gas is required.

Recently, simple gas measurement methods based on acoustic signals have been proposed: the detection of hydrogen leakage by acoustic signals [1] and the detection of oxygen gas concentration [2]. The average molecular weight of gas changes when hydrogen leaks or oxygen concentration changes, which results in the change of sound velocity and resonant frequency of acoustic sound.

We're also developing a new sensing method to measure gas molecular weight using acoustic signals from two whistles [3][4]. Previous studies have demonstrated the basic principles and fundamental experimental results; however, they have not evaluated the impact of temperature [3],[4]. It remains uncertain whether temperature has only a negligible influence on these characteristics, or if other factors, such as changes in the whistle's characteristics with varying temperatures, might also play a role in the observed outcomes. In this paper, we experimentally evaluated the effect of temperature. Furthermore, gas measurement of unknown molecular weight was tested using gases from cattle rumen fluid.

DOI: 10.5162/EUROSENSORSXXXVI/OT6.80

Sensing mechanism [3][4]

The proposed sensing mechanism of gas molecular weight using whistles is shown in Fig. 1. The fundamental frequency *f* when gas flows into the whistle can be expressed by the following:

$$f = a\sqrt{\frac{kRT}{M}} + bQ + c \qquad (1)$$

where *M*, *Q*, and *T* are the molecular weight, flow rate, and temperature of the gas, respectively, and *k* and *R* are the specific heat ratio and gas constant. The *a* is a whistle-specific constant, and the *b* and *c* are constants determined by the type and combination of whistles. The gas's molecular weight and flow rate can be calculated from each whistle's multiple frequency measurement results.

From above equation, changes in temperature are expected to be theoretically calculated. However, temperature *T* may affect the specific heat ratio *K* and the properties of the whistles themselves and cause further errors. Therefore, we will attempt to evaluate the experimental effect of temperature *T* on this study.

Experiment methods

The shapes of the whistles used in this study are shown in Fig. 2. Two whistles with different sizes

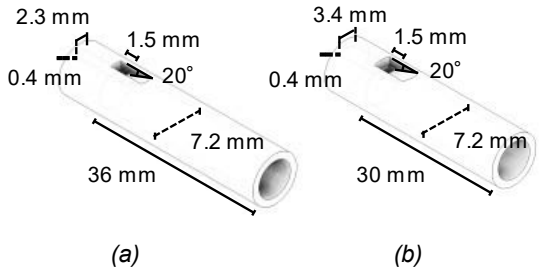

(a) *(b)*

Fig. 2. The images of the used two whistles. (a) Whistle 1, (b) Whistle 2.

were fabricated by a 3D printer (Keyence Corporation, Agilista) using acrylic UV curable resin (Keyence Corporation, AR-M2).

The frequency shift by temperature was evaluated by inserting two types of gases (N_2: molecular weight 28 and CO_2: molecular weight 44) with different temperatures from 22 to 28°C to each whistle. The sounds generated by the whistles were measured by a microphone (Ono Sokki Co., Ltd., MI-1271), and fundamental frequency was obtained.

As a demonstration, we also attempted to gas measurement of unknown molecular weight. With cattle breath analysis in mind, the molecular weight of the gas generated from cattle rumen fluid was collected and measured using the proposed method. For reference, the gas was also measured by using gas chromatograph (SHIMADZU CORPORATION, GC-2014) to know the actual molecular weight.

Experimental results

Figure 3 shows the effect of the temperature on each whistle in the case of measuring N_2 gas. It shows that the frequency is almost linear with the change in temperature, meaning that the effect of temperature is expected to be theoretically calculated. Because the experiment was conducted using plastic materials, which are considered susceptible to thermal effects, it seems that there is a theoretical possibility of compensating for temperature.

Noted that a change of 1 °C in temperature (which corresponds to an approximate 0.03 change in sqrt(T)) means that the frequency changes by 2-3 Hz/°C. It corresponds to the molecular weight change of around 0.03/°C, almost consistent with the theory. Though improvement of the accuracy to the molecular weight is the first requirement because it is still around 0.45 [4], theoretical temperature compensation is needed for accuracy measurement in the future

Figure 4 shows the measurement result of unknown gas generated from rumen liquid. The molecular weight error was at least less than 1.5. We intend to enhance the sensitivity further by refining the whistle in future experiments.

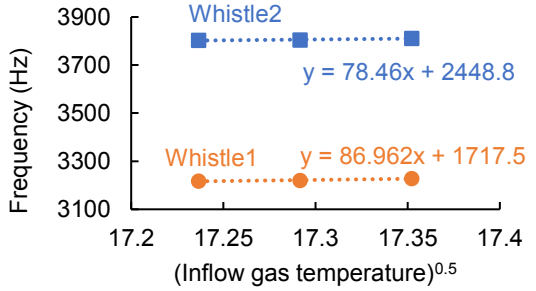

Fig. 3. Effect of temperature on the fundamental frequency of each whistle in case of N_2 gas.

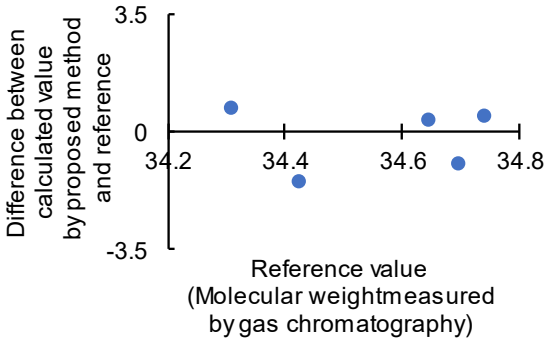

Fig. 4. The measurement result of unknown gas collected from rumen liquid.

Conclusions

We revealed that the effect of temperature can theoretically compensated in the proposed measurement method of the molecular weight of gas using whistles. The effect of temperature on the molecular weight was around 0.03/°C, which almost consistent with the theory. Furthermore, measurement of gas with unknown molecular weight was demonstrated, and the molecular weight resolution was at least less than 1.5. Noted that the sensitivity could be further improved by improving the measurement system and the whistle.

Acknowledgments

We appreciate Prof. S. Koike at Hokkaido University for his support. Part of this work was supported by JSPS KAKENHI Grant Number JP22K18778 and the Precise Measurement Technology Promotion Foundation.

References

[1] T. Okubo, S. Kijimoto, K. Matsuda and Y. Koba, *The Japan Society of Mechanical Enginerrs*, 75, no. 752, 912-918 (2009). (in Japanase)

[2] J. Wang, M. Chen, Q. Chen, H. Wang, *IEEE Sensors Journal*, 22, no. 21, 21281-21286 (2022).

[3] R. Yoshioka, M. Yamamoto, S. Takamatsu, T. Itoh, Proceedings in *2023 IEEE SENSORS*, Vienna, Austria, 1-4 (2023).

[4] R. Yoshioka, M. Yamamoto, S. Takamatsu, T. Itoh, *IEEJ Transactions on Sensors and Micromachines*, Accepted. (in Japanese)

DOI 10.5162/EUROSENSORSXXXVI/OT6.85

Plant on a Chip: Paper Fluidics for Spatio-Temporal Root Exudate Analysis

Daniel Patko[1,], Sepideh Izaddoust[1,2], Lionel X. Dupuy[3,4], Lourdes Basabe-Desmonts[2,4] and Fernando Benito-Lopez[1,*]*

[1]Microfluidics Cluster UPV/EHU, Analytical Microsystems & Materials for Lab-on-a-Chip Group, Analytical Chemistry Department, University of the Basque Country UPV/EHU, Leioa, Spain

[2]Microfluidics Cluster UPV/EHU, BIOMICs microfluidics Group, Lascaray Research Center, University of the Basque Country UPV/EHU, Vitoria-Gasteiz, Spain

[3]NEIKER, Derio, Spain

[4]IKERBASQUE, Basque Foundation for Science, Bilbao, Spain

*daniel.patko@gmail.com, fernando.benito@ehu.eus

Summary:

In order to develop a sustainable agriculture it is essential to use natural processes. Root exudates can attract beneficial microbes, increase the nutrient uptake from the soil and they can be a good indicator of the plant's stress responses. Unfortunately, the commonly used exudate collection methods cannot provide spatially and temporally detailed information. We developed a novel, wax patterned paper based microfluidic system to extract root exudates spatially and temporally. Using an integrated colorimetric glucose sensor we could reveal phenotypic differences between wheat varieties.

Keywords: Plant-on-a-chip, Paper-fluidics, Root exudates, Wax printing, Colorimetric detection

Background, Motivation and Objective

Our modern agriculture is far from being sustainable. A huge amount of the applied agrochemicals, such as fertilisers, leach into the environment [1,2] making an economic loss and an environmental damage. Using natural processes, like microbial interactions can address this challenge.

Soil microbiota has an undeniable role in the life of a plant. Microbes can increase its stress resilience or improve its nutrient uptake [3] . Using these interactions as plant fertilizers can decrease the ecological impact of agriculture, however we lack of essential knowledge regarding the nature of these processes. It is known that plants exude a wide range of molecules, such as sugars, to attract beneficial microorganisms [3,4], but the time dependency of this process is unknown, especially on single plant level.

The traditional way to detect root exudates is a labour active, time-consuming process, including purification steps and it requires trained personnel and a growth facility for the plants [5].

We developed an easy to use, cost-effective, modular, wax printed paper-based microfluidic system to overcome the above mentioned limitations (Figure 1). The developed chip is able to extract root exudates from a defined part of the root system, and able to follow the exudation changes over time. Moreover, it is possible to follow these changes on the single plant level.

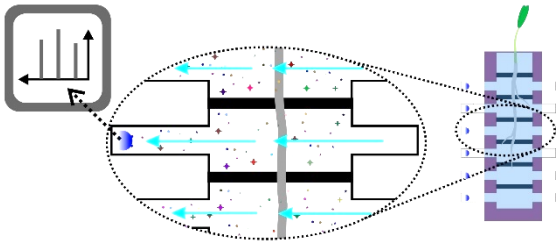

Figure 1: Scheme of the developed paper based microfluidic system for the investigation of root exudates. The exuded molecules can be delivered to the sensors using a flow generated by evaporation. The different root segments can be analyzed individually over time.

Description of the new System

The developed microfluidic system consists of a wax printed filter paper, a microscope slide and a polydimethylsiloxane (PDMS) slide. The wax is melted into the fiber structure of the filter paper creating hydrophobic barriers forming horizontal channels in parallel (Figure 2). The paper is also the growth substrate for the plant. For the experiments, as a relevant crop, we used wheat (*Triticum aestivum*).

An integrated a colorimetric TiO_2-alginate hydrogel based glucose sensor, developed by us [6],

was integrated at the outlet part of the paper channels to detect the exuded glucose by the plant root (Figure 2 right, picture).

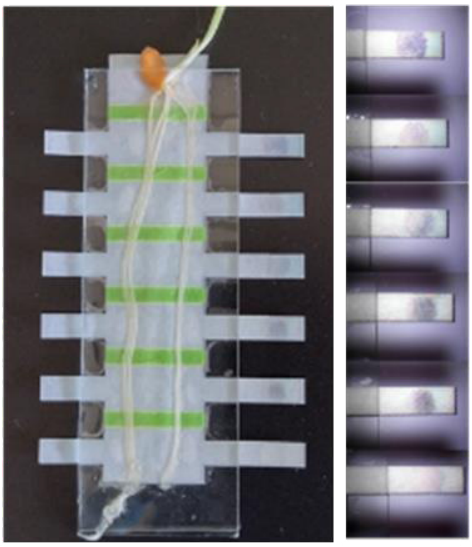

Figure 2. Picture of the microfluidic system with integrated glucose sensors (left) and magnified image of the sensors after exudate extraction (right). The colorimetric TiO_2-alginate hydrogel based glucose sensor clearly shows different colour intensities at different positions of the root.

Results

Using the developed patterned paper based microfluidic system the exuded glucose, by the root system, was detected and, along the root, we could capture the intensity differences in exudation. Moreover, glucose concentrations were determined colorimetrically and it was possible to differentiate between the exudation activity at different positions of root (Figure 3.).

Our method was capable to show, that the exudation starts at the top part of the root and with ageing, the younger parts are getting active too.

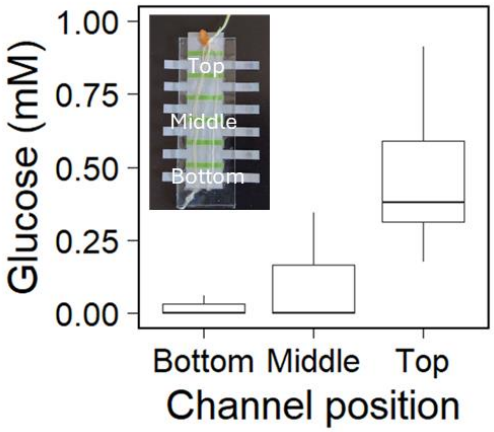

Figure 3. Graph presenting the produced amount of glucose during the 7 days of observation at different parts of the root system.

Acknowledgements

This work was supported by the European Commission's EXCELLENT SCIENCE - Marie Skłodowska-Curie Actions program, RhizoSheet MSCAIF, grant agreement number: 101028242. The "Ministerio de Ciencia y Educación de España" paña" under grant PID2020-120313GB-I00/AIE/10.13039/501100011033 y por FEDER una manerade hacer Europa, the Basque Government (Grant IT1633-22) and Proyecto de Investigación Fundamental Colaborativa – Investigación Fundamental ELKARTEK: KK-2023/0007.

References

[1] N. Beaudoin, J.K. Saad, C. Van Laethem, J.M. Machet, J. Maucorps, B. Mary, Nitrate leaching in intensive agriculture in Northern France: Effect of farming practices, soils and crop rotations, Agric Ecosyst Environ 111 (2005) 292–310. https://doi.org/10.1016/j.agee.2005.06.006.

[2] S. Delin, M. Stenberg, Effect of nitrogen fertilization on nitrate leaching in relation to grain yield response on loamy sand in Sweden, European Journal of Agronomy 52 (2014) 291–296. https://doi.org/10.1016/j.eja.2013.08.007.

[3] S.A. Rolfe, J. Griffiths, J. Ton, Crying out for help with root exudates: adaptive mechanisms by which stressed plants assemble health-promoting soil microbiomes, Curr Opin Microbiol 49 (2019) 73–82. https://doi.org/10.1016/j.mib.2019.10.003.

[4] J. Sasse, E. Martinoia, T. Northen, Feed Your Friends: Do Plant Exudates Shape the Root Microbiome?, Trends Plant Sci 23 (2018) 25–41. https://doi.org/10.1016/j.tplants.2017.09.003.

[5] A. Williams, H. Langridge, A.L. Straathof, G. Fox, H. Muhammadali, K.A. Hollywood, Y. Xu, R. Goodacre, F.T. de Vries, Comparing root exudate collection techniques: An improved hybrid method, Soil Biol Biochem 161 (2021) 108391. https://doi.org/10.1016/j.soilbio.2021.108391.

[6] U.B. Gunatilake, S. Garcia-Rey, E. Ojeda, L. Basabe-Desmonts, F. Benito-Lopez, TiO2Nanotubes Alginate Hydrogel Scaffold for Rapid Sensing of Sweat Biomarkers: Lactate and Glucose, ACS Appl Mater Interfaces 13 (2021) 37734–37745. https://doi.org/10.1021/acsami.1c11446.

DOI 10.5162/EUROSENSORSXXXVI/OT6.89

Fabrication of Nanochannels with Funnel-like Inlet Structures for the Analysis of Single DNA Molecules

Nicole Hintz[1,2], Christopher Johnson[3], Martina Hübner[1]
[1] Robert Bosch GmbH, Robert-Bosch-Campus 1, Renningen, Germany
[2] Institute for Microsensors, -actuators and -systems (IMSAS), Otto-Hahn-Allee 1, Bremen, Germany
[3] Robert Bosch LCC, 384 Santa Trinita Avenue, Sunnyvale, Ca, USA

E-mail address: nicole.hintz@de.bosch.com

Summary:
A new fabrication method for realizing fluidic nanochannels with funnel-like inlet structures in silicon technology is presented. Nanochannels are a useful tool for DNA analysis since the molecules must first be linearized to enter the nanochannels and the linearization is a prerequisite for DNA mapping or sequencing. Inlet structures, like funnels, help guiding the DNA and bringing it into the channels. The nanochannels demonstrated in this work are realized using standard MEMS processes and photolithography, enabling cheap and scalable production for a wide range of biotechnology applications.

Keywords: Nanochannel, Inlet structure, Funnel, MEMS Fabrication, DNA Analysis

Background and Motivation

Micro-biosensors bring many benefits through their miniaturization [1]. Micro- and nanoscale features allow manipulation of single cells or even molecules and the integration of their analysis on lab-on-chip systems. The sequencing and mapping of single DNA molecules is made possible by the linearization of single DNA molecules inside of a nanochannel [2]. When the dimensions of a structure are smaller than the persistence length of DNA, the DNA is forced to extend instead of the entropically-favorable coiled state, as sketched in figure 1. The negatively charged DNA can be pulled into a nanochannel by an electric field. Nevertheless, inserting the DNA into the channels is challenging. To change its conformation from coiled to linear the so-called entropic barrier has to be overcome [3].

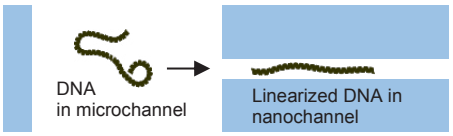

Fig. 1. Schematic of linearized DNA inserted into a nanochannel

Adding a funnel-like inlet to the nanochannel creates a gradient between the volume in front of the nanochannel and the channel itself, which makes the overcoming of the entropic barrier easier and lowers the needed electrical force [3]. A funneled inlet can also increase the capture rate of molecules in the channel and avoid hairpin formation and clogging of nanochannels [2,4].

Therefore, creating nanochannels with funnel-inlets with a cheap and scalable process is vital for the fabrication of DNA analysis systems. However, the fabrication of nanostructures poses challenges. Since the standard fabrication processes for microsystems are limited by the wavelength of the light used for photolithography structures smaller than 1 µm are difficult to achieve. There are methods to overcome this, like deep-UV lithography or electron beam lithography. A different method is focused ion beam milling (FIB) to directly create the nanostructures or a stamp to use in nanoimprint lithography (NIL). These mentioned methods are expensive and often not scalable [1]. To circumvent these expensive methods and the limit of photolithography, certain workarounds can be used to create nanostructures only with standard fabrication processes. For example, nanochannels can be fabricated by thin-film evaporation and etching of a sacrificial layer [5]. But the addition of funnel inlet structure to the channels is only reported in systems fabricated with NIL or FIB [2,3,4], and not for structures fabricated using only standard processes. Such a process was investigated for the first time and will be discussed here.

Description of the New Fabrication Method

The fabrication of long nanochannels with horizontal funnel-shaped inlet structures to facilitate the analysis of DNA molecules is shown schematically in Figure 2. The nanochannel is

created by selectively under-etching a sacrificial layer under a top layer. Therefore, the channel dimensions depend on the thickness of the sacrificial layer and the under etch time. The channel is then closed by a capping layer. Microchannels, that contact the nanochannels, are etched with an anisotropic process. To fabricate the funnel-shaped inlets of the channels, an additional etch step is added, which etches the material next to the nanochannel faster at the entrance than the inside of the channel. This step creates a horizontal funnel inlet.

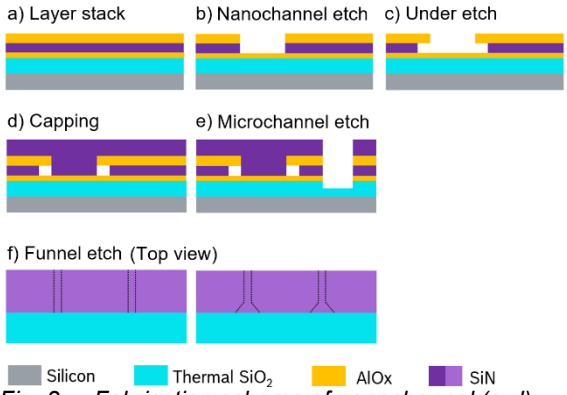

Fig. 2. Fabrication scheme of nanochannel (a-d), microchannel (e) and funnel-inlet (f).

Results

Nanochannels with a length of 50 µm have been fabricated, but channels with lengths up to several millimeters are possible with this fabrication method since the length is not the limiting factor in the fabrication. A cross section of a channel with a width of 250 nm and a height of 40 nm is displayed in figure 3.

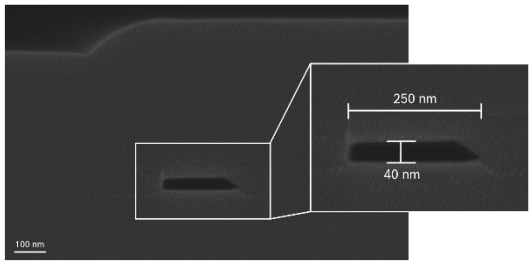

Fig. 3. Electron microscope picture of a nanochannel cross section with its dimensions.

The existence of a continuous nanochannel can be demonstrated with the help of a fluorescent solution. The solution is introduced in the upper microchannel, then fills the nanochannels by capillary forces and reaches the lower microchannel (see figure 4).

Different funnel inlet sizes can be created by varying the duration of etch step, with the funnel inlet getting larger and the angle shallower with increasing time, as seen in figure 5. The inlet size widens from roughly 200 nm nanochannel width to 1 µm. The influence of other parameters of the etch step on the funnel shape, like

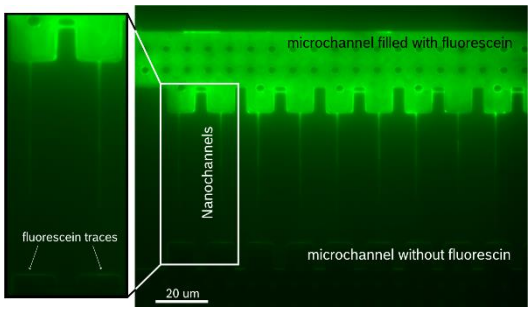

Fig. 4. Picture of a microchannel with several nanochannels. The fluorescein solution added in the upper microchannel got through the nanochannels into the lower microchannel.

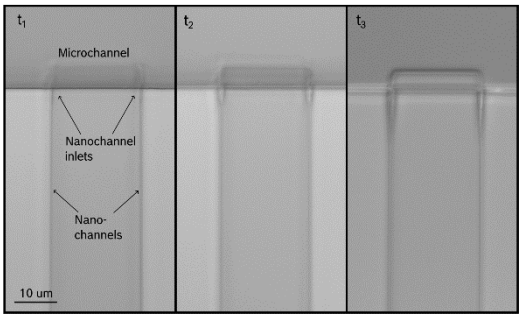

Fig. 5. Picture of funnel inlet shapes after different etching times ($t_1 < t_2 < t_3$).

pressure and flow rate of the etchant will be tested to create inlets with arbitrary shapes.

In conclusion, it can be said that nanochannels with inlet structures of different sizes have been successfully fabricated. The size of the inlets can be varied by the duration of the etch step. Inlet sizes of 1 µm have been created for a 200 nm wide channel.

This work was supported by BMBF FKZ 03ZU1208BH: nanodiag BW.

References

[1] J. O. Tegenfeldt *et al.*, Micro- and nanofluidics for DNA analysis, *Anal. Bioanal. Chem.* 378 (7), 1678–1692, (2004), doi: 10.1007/s00216-004-2526-0

[2] J. Wu *et al.*, Engineering inlet structures to enhance DNA capture into nanochannels in a polymer nanofluidic device produced via nanoimprint lithography, *Micro Nano Eng.* 21 (2023), doi: 10.1016/j.mne.2023.100230

[3] J. Zhou *et al.*, Enhanced nanochannel translocation and localization of genomic DNA molecules using three-dimensional nanofunnels, *Nat. Commun.* 8 (2017), doi: 10.1038/s41467-017-00951-4

[4] F. M. Esmek *et al.*, Sculpturing wafer-scale nanofluidic devices for DNA single molecule analysis, *Nanoscale* 11, 13620–13631 (2019), doi: 10.1039/C9NR02979F

[5] H. T. Hoang *et al.*, Wafer-scale thin encapsulated two-dimensional nanochannels and its application toward visualization of single molecules, *J. Colloid Interface Sci.* 367, 455–459, (2012), doi: 10.1016/j.jcis.2011.10.00

DOI 10.5162/EUROSENSORSXXXVI/OT6.97

Electroporation Monitoring by Machine Learning and Single Cell Morphodynamic on Lab-on-Chip

Gianni Antonelli[1], Francesca Camera[2], Arianna Mencattini[1], Arianna Casciati[2], Mirella Tanori[2], Alessandro Zambotti[2], Giorgia Curci[1], Joanna Filippi[1], Michele D'Orazio[1], Paola Casti[1], Caterina Merla[2], Eugenio Martinelli[1]

[1] Department of Electronic Engineering & Interdisciplinary Center for Advanced Studies on Lab-on-Chip and Organ on-Chip Applications, University of Rome Tor Vergata; Via del Politecnico,1; Rome (Italy)

[2] Division of Health Protection Technologies, Italian National Agency for Energy, New Technologies and Sustainable Economic Development (ENEA); Via Anguillarese, 301; Rome (Italy)

Corresponding Author's e-mail address: g.antonelli@ing.uniroma2.it

Summary:

Electroporation is a reliable, reproducible technique to induce biological cell membrane poration. Because of the biological and clinical interest in this technique, recently, many Lab-On-Chip platforms have been proposed to understand more about deep electroporation mechanisms. This led to the discovery of many electroporation side effects, such as cell contractivity and blebbing. In this work, we propose a new sensing system based on Lab-On-Chip and machine learning to correlate these side effects observed by brightfield time-lapse microscopy with electroporation efficiency.

Keywords: Electroporation, Lab-On-Chip, Machine Learning, Time-Lapse Microscopy,

Background, Motivation and Objective

Since its discovery in 1968, electroporation spread its applicability in biological and clinical research [1]. Delivering high electric fields on a biological tissue for short periods, usually nanoseconds or microseconds, permits the generations of nanopores on cells. Changing these parameters guarantees great flexibility of the technique in multiple applications, spanning electrochemotherapy, cell lysis, fusion, or bacteria inactivation.

Even though electroporation has been known for a long time, its inner mechanisms are still under study. For example, from the morphological point of view, it was discovered that cells react to the electric field application by contracting and blebbing [2].

These findings were significantly made possible by the slight transition in studying these phenomena from classical biological support (e.g., culture dishes) to Lab-On-Chip platforms, which allow the set-up of more complex experiments in a minimal environment.

Information extracted from these devices can sometimes be challenging to analyze without using more complex models, such as machine learning algorithms. Particularly in microscopy image analysis, these models permit extracting hidden features and intricate trends that are impossible to catch quantitatively by hand.

In this work, we present a sensing system based on a low-cost Lab-On-Chip platform able to correlate the electroporation efficiency with its side effects by applying a tailored machine learning algorithm on brightfield time-lapse microscopy images.

Method description

A Lab-On-Chip based on transferred Laser-Induced-Graphene (LIG) was designed and fabricated using a technique we recently proposed [3]. Briefly, LIG electrodes are first generated by laser scribing a polyimide sheet. Then, the printed geometries are transferred to a transparent, biocompatible PMMA substrate by surface solubilization.

The chip exhibited six pairs of interdigitated electrodes with different pitches, used to stimulate the U-87 glioblastoma cell line with several voltages and electric fields (Fig. 1). During the stimulation, fluorescence and brightfield time-lapse microscopy monitored calcium intake and cell contractility, respectively.

A custom machine-learning algorithm based on Particle Image Velocimetry (PIV) and cell segmentation computed single-cell contractivity and

internal calcium quantity tracking during the time-lapse [4].

Finally, the extrapolated peaks of cumulative velocity were thresholded and used to estimate the electroporation efficiency in the acquired frame. Similarly, we used the detected calcium intake spikes as the ground truth, calculating the real electroporation efficiency.

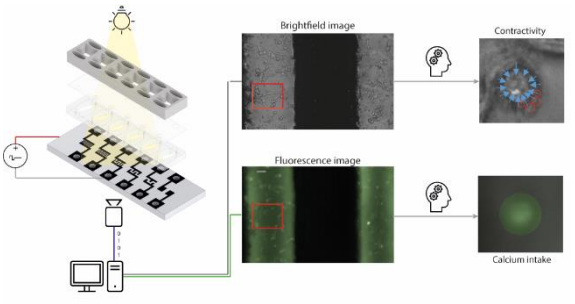

Fig.1. A Lab-On-Chip is designed to have six different interdigitated electrodes and separated chambers for cell culture. Each electrode pair is connected to a high-voltage pulse generator. Fluorescence and brightfield time-lapse microscopy are acquired at the same time. Each time-lapse frame is then analyzed using a tailored machine, computing cell contractivity and calcium intake.

Results

To better understand the behaviour of cell culture after electroporation, it was necessary to study cell movements and calcium presence before the stimulus. As expected, cells exhibited an independent movement, which was necessary to subtract from the one induced by the electric field application. Moreover, U-87 cells were demonstrated to contain a significant amount of calcium ions in their cytoplasm also before the poration stimulus.

Once the pulsed electric field was applied, cells started to contract and bleb, generating a peak in contraction detected by PIV. Calcium diffusion was observed to be almost instantaneous, while cell contractivity follows a second-scale dynamic. Moreover, as expected, the beginning of cell contractivity perfectly correlates with the fluorescence peak induced by calcium intake caused by cell poration (Fig. 2a).

Finally, velocity and fluorescence peaks from single cells were then separately thresholded and used to compute the electroporation efficiency of the experiment. As can be evinced from Fig. 2b, there is an almost complete correspondence between the efficiency computed by fluorescence and the one calculated from contraction ($R^2 = 0.931$ around the bisector). Moreover, these results were obtained by aggregating data from different electrodes and electric fields. This indicates that our sensing system can predict electroporation from brightfield time-lapse microscopy without additional fluorescent channels independent of the experimental conditions.

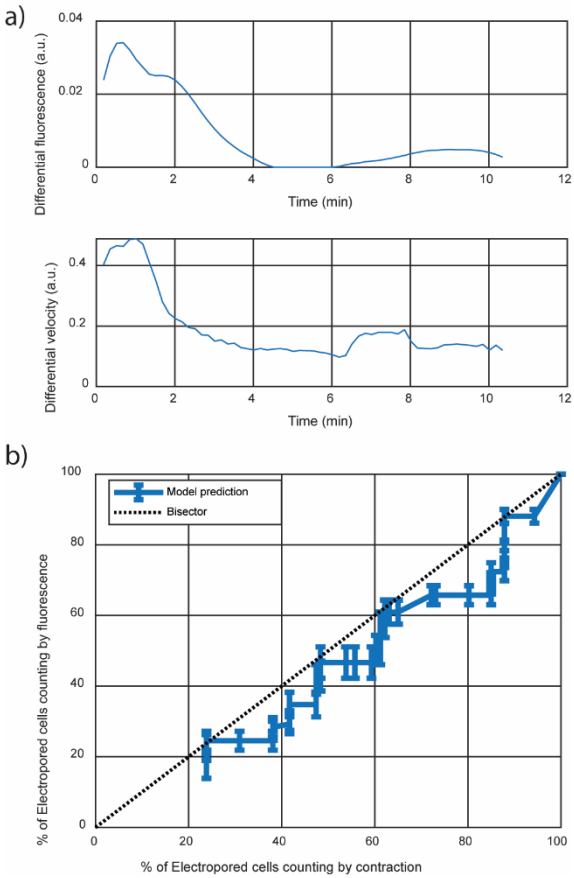

Fig 2. a) Fluorescence intensities from single cells during the time-lapse experiments are compared with the contractivity velocity calculated by PIV analysis. b) Average fluorescence intensity is correlated with the peak velocity. Cell population heterogeneity and different electrode geometries contribute to performance variability.

References

[1] T. F. Justesen, A. Orhan, H. Raskov, C. Nolsoe, and I. Gögenur, “Electroporation and Immunotherapy—Unleashing the Abscopal Effect,” *Cancers 2022, Vol. 14, Page 2876*, vol. 14, no. 12, p. 2876, Jun. 2022, doi: 10.3390/CANCERS14122876.

[2] P. M. Graybill, A. Jana, R. K. Kapania, A. S. Nain, and R. V. Davalos, “Single Cell Forces after Electroporation,” *ACS Nano*, vol. 15, no. 2, pp. 2554–2568, Feb. 2021, doi: 10.1021/ACSNANO.0C07020.

[3] G. Antonelli *et al.*, “Laser-Induced Graphene Wet Transfer Technique for Lab-On-Chip Applications,” Submitted

[4] G. Antonelli *et al.*, “A Lab-On-Chip sensing system for electroporation based on brightfield time-lapse,” Submitted

DOI 10.5162/EUROSENSORSXXXVI/OT6.111

DEVELOPMENT OF AN ISFET-BASED SYSTEM FOR GENETIC DETECTION OF LEUKEMIA ONCOGENE

Léony S. Oliveira[1], Norma Lucena-Silva[2], Marie Hangouët[3], Cesar A.S. Andrade[4], Maria D.L. Oliveira[4], Joan Bausells[5], Norman Pfeiffer[6], Nadia Zine[3], Abdelhamid Errachid[3]

[1] Programa de Pós-Graduação em Inovação Terapêutica, Universidade Federal de Pernambuco, 50670-901 Recife, PE, Brazil,

[2] Instituto Aggeu Magalhães, Fundação Oswaldo Cruz (Fiocruz), 50670-420 Recife, PE, Brazil. Laboratório de Biologia Molecular, Departamento de Oncologia Pediátrica, Instituto de Medicina Integral Professor Fernando Figueira (IMIP), 50070-550 Recife, PE, Brazil.

[3] Institute of Analytical Sciences (ISA) – UMR 5280, French National Center for Scientific Research (CNRS), 69100, Lyon, France.

[4] Laboratório de Biodispositivos Nanoestruturados, Departamento de Bioquímica, Universidade Federal de Pernambuco, 50670-901 Recife, PE, Brazil

[5] Fraunhofer IIS, Fraunhofer Institute for Integrated Circuits IIS, Am Wolfsmantel 33, Erlangen, 91058, Germany.

[6] Instituto de Microelectrónica de Barcelona (IMB-CNM,CSIC), Campus UAB, 08193 Bellaterra, Spain.

Corresponding Author's e-mail address: leony.oliveira@ufpe.br, abdelhamid.errachid-el-salhi@univ-lyon1.fr

Summary:

A Point-of-care device was developed using Ion-selective field-effect transistors (ISFETs) for real-time detection of molecular targets, eliminating the requirement for a highly controlled environment. This device successfully detected the translocation between chromosomes 12 and 21 (t(12;21)), which is one of the most common mutations associated with childhood acute lymphoblastic leukemia (ALL).

Keywords: ISFET, leukemia, point-of-care, potenciometry, genosensor.

Title

Development of an isfet-based system for genetic detection of leukemia oncogene.

Introduction

Acute lymphoblastic leukemia (ALL) is the most common childhood cancer, accounting for approximately 25% of cancer diagnoses. Accurate determination of the genetic mutations associated with leukemia is crucial for patient prognosis. One of the most recurrent mutations in ALL is the translocation between chromosomes 12 and 21 (t (12;21)) [1]. Current genetic diagnostic methods, such as fluorescence in situ hybridization (FISH) and reverse transcription quantitative polymerase chain reaction (RT-qPCR), are efficient in detecting these mutations. However, they often require lengthy experimental protocols and a highly controlled laboratory environment [2]. In contrast, point-of-care devices enable real-time detection of molecular targets without the need for a highly controlled environment. Ion-selective field-effect transistors (ISFETs) are miniaturized devices that can be utilized for genetic analysis through the hybridization of complementary DNA sequences [3].

Objective

In this study, we developed an ISFET-based system for the detection of t (12;21) in the pediatric population.

Methods

Therefore, the ISFET system was used for the detection of genetic markers in childhood ALL that had never been studied before in biosensors field (Fig.1a). For this The ISFET was initially characterized using different pH buffers to assess its ionic selectivity. Subsequently, the ISFET was coated with a layer of TESUD, and a specific DNA probe for t (12;21) was immobilized on its surface. The biorecognition process was evaluated through hybridization tests with plasmid samples at various concentrations. Potentiometry was employed to characterize all steps of the process.

Results and Discussion

The ISFET exhibited a decrease in drain-to-source current (I_{DS}) plateau with an increase in

pH (Fig.1b). In addition, the threshold potential (V_T) increased with higher pH levels, indicating the system's sensitivity to ion concentration (Fig.1c) [3].

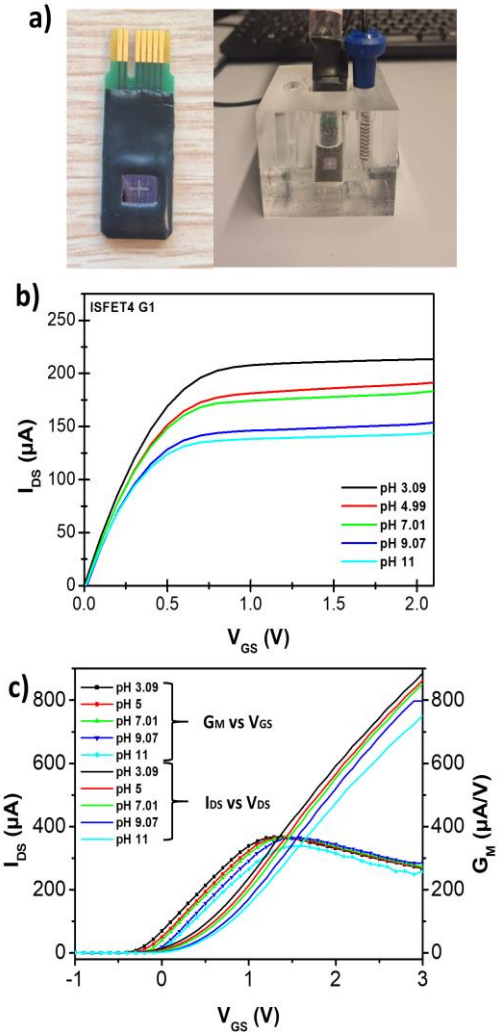

Fig. 1. ISFET system (a) and influence of pH on I_{DS} (b) and V_T (c) ISFETpH 3.09, 4.99, 7.01, 9.07 and 11.

In the hybridization tests, an increase in V_T and were observed with increasing sample concentrations in the same pH buffer, suggesting successful biorecognition through the hybridization process. This occurs because DNA is negatively charged due to phosphate groups in its structure. Thus, the hybridization process of the onto the ISFET increases the fixation of negative charge on the surface, leading to a change in the gate potential [4] In addition to surface charge alteration, the DNA hybridization process can also cause ionic redistribution in the medium [4]. Thus, a good linearity of response was achieved by correlating ΔV_T x Plasmid Concentration, indicating the system's detection sensitivity (Fig.2b).

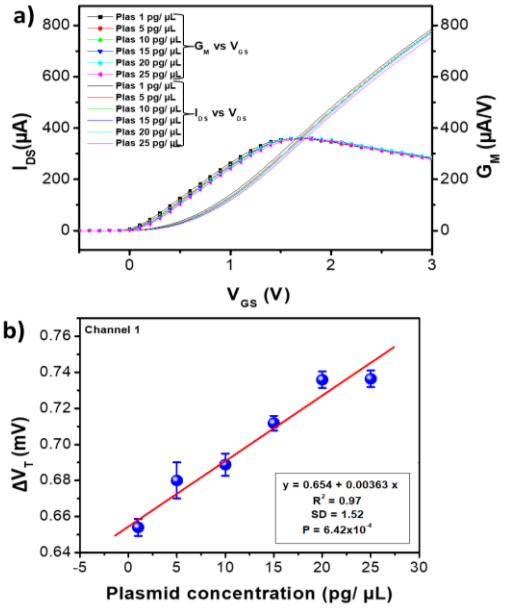

Fig. 2. Influence of hybridization on ISFET (a) and linear plot assays of V_T variation of ISFET (b).

Conclusion

The evaluated ISFET-based systems demonstrated promising performance for genetic detection of leukemic oncogenes, offering potential applications in clinical settings.

References

[1] S. K. Tasian, M. L. Loh and S. P. Hunger, Childhood acute lymphoblastic leukemia: Integrating genomics into therapy,*Cancer* 121, 3577-90 (2015); doi: 10.1002/cncr.29573.

[2] T. Pincez, R. Santiago, H. Bittencourt, I. Louis, M. Bilodeau, A. Rouette, L. Jouan, J. R. Landry, F. Couture, J. Richer, P. Teira, M. Duval and S. Cellot, Intensive monitoring of minimal residual disease and chimerism after allogeneic hematopoietic stem cell transplantation for acute leukemia in children,*Bone Marrow Transplant* 56, 2981-2989 (2021); doi: 10.1038/s41409-021-01408-5.

[3] H. Ben Halima, F. G. Bellagambi, F. Brunon, A. Alcacer, N. Pfeiffer, A. Heuberger, M. Hangouet, N. Zine, J. Bausells and A. Errachid, Immuno field-effect transistor (ImmunoFET) for detection of salivary cortisol using potentiometric and impedance spectroscopy for monitoring heart failure,*Talanta* 257, 123802 (2023); doi: 10.1016/j.talanta.2022.123802.

[4] H. Kawarada and A. R. Ruslinda, Diamond electrolyte solution gate FETs for DNA and protein sensors using DNA/RNA aptamers,*physica status solidi (a)* 208, 2005-2016 (2011); doi: 10.1002/pssa.201100503.

DOI 10.5162/EUROSENSORSXXXVI/OT6.116

Ion-Sensitive Field Effect Transistor (ISFET)-Based DNA Detection for Enterotoxigenic *E. coli* (ETEC)

Mongkol Techakasikornpanich[1], *Duangporn Polpanich*[2], *Marie Hangouet*[3], *Joan Bausells*[4], *Norman Pfeiffer*[5], *Nadia Zine*[3], *Kulachart Jangpataraponsa*[1]*,*Abdelhamid Errachid*[3]*, *and Abdelhamid Elaissari*[3]

[1] *Center for Research Innovation and Biomedical Informatics, Faculty of Medical Technology, Mahidol University, Bangkok 10700 Thailand,*

[2] *National Nanotechnology Center (NANOTEC), National Science and Technology Development Agency (NSTDA), Pathum Thani 12120, Thailand,*

[3] *Universite Claude Bernard Lyon 1, ISA, UMR 5280, CNRS, 5 rue de la Doua, 69100 Villeurbanne, France,*

[4] *Instituto de Microelectrónica de Barcelona (IMB-CNM,CSIC), Campus UAB, 08193 Bellaterra, Spain*

[5] *Fraunhofer IIS, Fraunhofer Institute for Integrated Circuits IIS, Am Wolfsmantel 33, Erlangen, 91058, Germany*

Corresponding Author's e-mail address:
kulachart.jan@mahidol.ac.th (Kulachart Jangpataraponsa),
abdelhamid.errachid-el-salhi@univ-lyon1.fr (Abdelhamid Errachid)

Summary:

In this study, we demonstrate novel bacterial detection using DNA hybridization-based electrochemical biosensors for enterotoxigenic *Escherichia coli* (ETEC). The ion-sensitive field-effect transducer (ISFET) was immobilized with LT-probe, which is specifically for the heat-labile gene of ETEC. Potentiometric measurement and Electrochemical impedance spectroscopy (EIS) are performed to improve the successful development of the detection of ETEC, which represents a promising technique for rapid and sensitive bacterial detection.

Keywords: ISFET biosensors, DNA-based biosensors, ETEC, Bacterial detection, DNA hybridization

Background

Enterotoxigenic Escherichia coli (ETEC) is foodborne pathogenic bacteria, that causes cholerae-like diarrhea in children younger than 5 years old. Due to the fecal-route infection, ETEC can be transmitted via contaminated food and beverage. The detection of ETEC is commonly identified by molecular-based detection, such as polymerase chain reaction (PCR) and real-time PCR (qPCR), which use a heat-labile toxin (LT) gene as a target. Although these methods are highly sensitive and specific to ETEC, they require expensive equipment and well-trained staff. Moreover, they may require an enrichment process, which is time-consuming [1], [2], [3]. Thus, the development of rapid, easy, and point-of-care (POC) detection is a challenge for bacterial detection. In recent years, ion-sensitive field effect transducer (ISFET)-based biosensors have gained interest in the fields of detection, due to miniaturization, cost-effectiveness, and high sensitivity [4], [5]. In this study, we developed a more rapid, highly sensitive, and highly specific DNA-based ISFET biosensor for the detection of ETEC contaminated in water.

Methods

The ISFET's surface was activated by UV/Ozone procleaner to modify hydroxyl groups on the surface and then were silanized with 11-(triethoxysilyl) undecanal (TESUD) by the vapor-phase method. After functionalization, the ISFET was placed in an oven at 100°C for 1h. The aminated-LT-probe was dropped and incubated overnight at 4°C. After that, the immobilized ISFET was rinsed with TE buffer pH 8 and dried with N_2. 1% Ethanolamine was dropped on the ISFET and incubated for 1 h at RT to block unspecific binding molecules. The DNA sample, extracted from ETEC, was heated for 5 min to denaturation of double-stranded DNA structure and incubated with the immobilized ISFET for 10 min. The ISFET was rinsed with PBS buffer pH 7.4 and dried with N_2. The potentiometry and electrochemical impedance spectroscopy (EIS) of the ISFET were determined using PBS buffer pH 7.4

Results

LT-probe immobilized ISFET was investigated by analyzing various concentrations of extracted DNA from ETEC ($1.9x10^{-5}$ to $1.9x10^{-1}$ µg/mL). Filtrate PBS was used as a negative control to provide the reference signal of the ISFET sensor. Potentiometry and EIS were measured in PBS solution pH 7.4. Fig. 1 demonstrates the responsible ISFET to various DNA samples, measured by drain current (I_{DS}) and transconductance (G_m) vs. gate-to-source voltage (V_{GS}) at drain-to-source voltage (V_{DS}) = 0.5 V. I_{DS} and G_m vs. V_{GS} have slightly shifted to the negative value when increasing the concentration of ETEC's DNA. The threshold voltage (V_T), extracted from I_{DS} and G_m vs. V_{GS}, demonstrated the decrease of V_T when increasing the bacterial concentration.

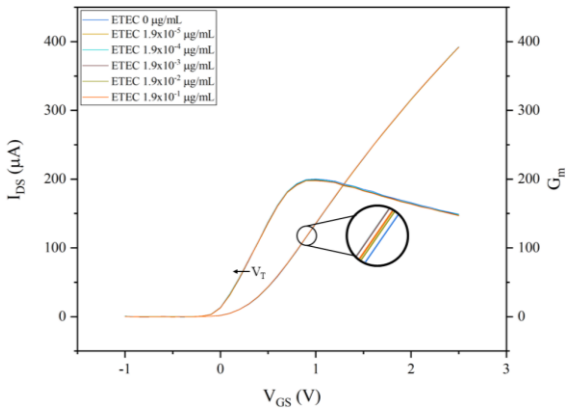

Fig. 1. I_{DS} and G_m vs V_{GS} obtained by analyzing ETEC's DNA samples in TE buffer ($1.9x10^{-5}$ to $1.9x10^{-1}$ µg/mL) at V_{DS} = 0.5 V.

Due to the narrow change of the potentiometric signal, EIS measurement was used to reach the sensitivity of the detection. The Nyquist plot of EIS at different concentrations of DNA samples ($1.9x10^{-5}$ to $1.9x10^{-1}$ µg/mL) decreased the charge transfer resistance on the modified ISFET surface, compared with the reference, ETEC 0 µg/mL, as shown in Fig 2.

These results improve the successful development of a label-free DNA-based ISFET sensor for the detection of ETEC's DNA using LT-probe.

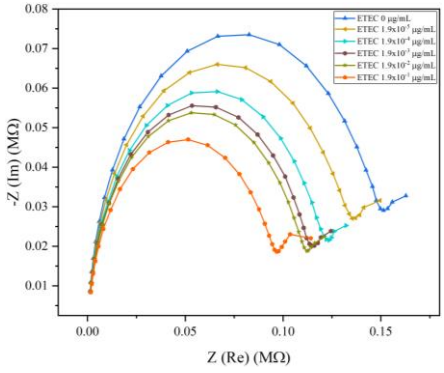

Fig. 2. Nyquist plots obtained by analyzing ETEC's DNA samples in TE buffer ($1.9x10^{-5}$ to $1.9x10^{-1}$ µg/mL). EIS frequency was ranged from 100 Hz to 200 KHz, with E_{ac} 100 mV and E_{dc} 0 V.

Conclusion

This work has proven the successful development of a DNA-based ISFET biosensor for the detection of heat-labile toxin gene which is specifically for ETEC. Potentiometry and EIS measurements were used to determine the efficiency of the ISFET sensor, which provided a decreasing trend when increasing the concentration of the DNA samples. It can represent the rapid detection of bacterial detection, which is a promising technique for point-of-care detection.

References

[1] K. Jangpatarapongsa, K. Saimuang, D. Polpanich, R. Thiramanas, M. Techakasikornpanich, P. Yudech, et al, Increased sensitivity of enterotoxigenic Escherichia coli detection in stool samples using oligonucleotide immobilized-magnetic nanoparticles, *Biotechnology Reports* 32, e00677 (2021); DOI: https://doi.org/10.1016/j.btre.2021.e00677

[2] Å. Lothigius, A. Janzon, Y. Begum, Å. Sjöling, F. Qadri, A. M. Svennerholm and I. Bölin, Enterotoxigenic Escherichia coli is detectable in water samples from an endemic area by real-time PCR, *Journal of Applied Microbiology* 104, 1128-1136 (2008); DOI: https://doi.org/10.1111/j.1365-2672.2007.03628.x

[3] S. Chakraborty, C. Harro, B. DeNearing, J. Brubaker, S. Connor, N. Maier, et al, Impact of lower challenge doses of enterotoxigenic Escherichia coli on clinical outcome, intestinal colonization and immune responses in adult volunteers, *PLOS Neglected Tropical Diseases* 12, e0006442 (2018); DOI: 10.1371/journal.pntd.0006442

[4] H. Ben Halima, F. G. Bellagambi, M. Hangouët, A. Alcacer, N. Pfeiffer, A. Heuberger, et al, A novel electrochemical strategy for NT-proBNP detection using IMFET for monitoring heart failure by saliva analysis, *Talanta* 251, 123759 (2023); DOI:https://doi.org/10.1016/j.talanta.2022.123759

[5] H. Ben Halima, F. G. Bellagambi, M. Hangouët, A. Alcacer, N. Pfeiffer, A. Heuberger, et al, A Novel IMFET Biosensor Strategy for Interleukin-10 Quantification for Early Screening Heart Failure Disease in Saliva, *Electroanalysis* 35, e202200141 (2023); DOI: https://doi.org/10.1002/elan.202200141

DOI 10.5162/EUROSENSORSXXXVI/OT6.132

Electropolymerization of porphyrinoids on LIG as EGFET-based sensor array for ascorbic acid detection

Kishore Pushparaj [1], Lorena Di Zazzo [2], Alexandro Catini [1], Rosamaria Capuano [1], Valerio Allegra [1], Gabriele Magna[2], Chiara Manganiello[1], Gianni Antonelli [1], Eugenio Martinelli [1], Roberto Paolesse [2], and Corrado di Natale [1]

[1] Department of Electronic Engineering, University of Rome Tor Vergata, 00133 Roma, Italy

[2] Department of Chemical Science and Technology, University of Rome Tor Vergata, 00133 Roma, Italy

Corresponding Author's e-mail address: dinatale@uniroma2.it

Summary:

Laser-induced graphene was obtained from polyimide films by lasing with a commercial CO_2 laser. Then porphyrinoids were electrosynthesized on the electrodes using cyclic voltammetry. These electrodes were employed as working electrodes in an extended gated field-effect transistor configuration. The array exhibits excellent sensitivity towards ascorbic acid and dopamine. Furthermore, artificial tears were tested with and without ascorbic acid as real samples.

Keywords: EGFET, laser-induced graphene, ascorbic acid, porphyrinoids, electrosynthesis.

1. Introduction:

L-ascorbic acid is a well-known water-soluble antioxidant present in many biological systems, and there are several ways to detect it [1]. ChemFET sensors are one of the recent interests in biological applications. Extended gate field effect transistor (EGFET) is quite modified from ion sensitive-FET sensors where the transducer is away from the electrolytic solution which gives the device long-term stability. Because MOSFETs are reusable in this technique, but the working electrode needs to be replaced, we need to pay attention to developing sensing materials. Preparation of electrodes is always a crucial part of the development of I sensors, where laser-induced graphene (LIG) is an easy method to obtain highly conductive graphene. Porphyrinoids are excellent ionophores materials that have been exploited in potentiometric sensors [2]. In this work, we electrosynthesized the porphyrinoids on laser-induced graphene (LIG) and used a sensor array using the EGFET technique to detect ascorbic acid in artificial tears.

2. Materials and methods:

A 125 µM polyimide sheet was lasered to produce LIG. The polyimide was cleaned with ethanol before laser illumination. Double lasing was performed with laser power of 10 W/cm2, at a rate of 20 cm/s and a resolution of 1000 PPI. The LIG obtained was used to electrosynthesis porphyrinoids in 0.1M TBAC. Electropolymerization was carried out as reported in our previous work [3]. This forms a sensor array consisting of 8 sensors: LIG, LIG/$Cu(NH_2)_3TPC$, LIG/ $Cu(NH_2)_3TPC\_LUT$, LIG/ $Co-PPh_3(NH_2)_3TPC$, LIG/ $Mn-Cl(NH_2)_3TPC$, LIG/ $Cu-5,10(NH_2)_2TPP$, LIG/ $5,15(NH_2)_2TPP$ and LIG/ $5,10(NH_2)_2TPP$ (left to right). Each electrode was connected to the gate terminal and a saturated calomel electrode was used to bias the gate as shown in Fig. 1. 100 µl of artificial tears (purchased from a pharmacy) were tested as a real sample in 1X PBS at.

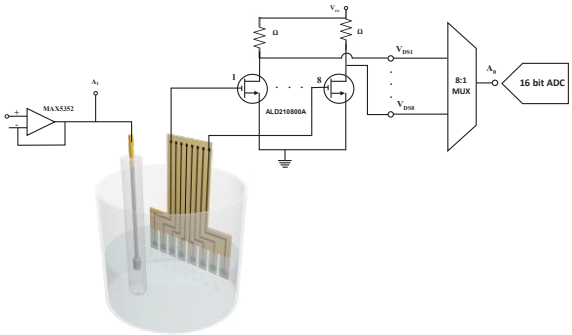

Figure 1. Schematic of the experimental setup.

3. Result and discussion:

Fig. 3 shows the principal component analysis (PCA) of the sensor array. The sensor was evaluated with ascorbic acid, dopamine, and artificial tears with and without ascorbic acid. The score plot shows the residual of the

repeated measurements. Fig 2 a) represents the scope plot of the sensor array based on ascorbic acid, dopamine, the mixture of dopamine and ascorbic, and synthetic tears with and without ascorbic acid Both PC1 and PC2 correspond to 97.77% of the total variance. The measurements were repeated twice with a two-sensor replica. Fig 3 b) Load plots indicate the execution of the sensor array where the sensor projects in different directions. It is noteworthy that Cu-5,10(NH_2)$_2$TPP is projected in the opposite direction with respect to the bare LIG electrode. On the other hand, LIG/ Cu(NH_2)$_3$TPC_LUT doesn't provide any information with respect to LIG. It is noticed that LIG contributes a lot more towards dopamine than electrosynthesized sensors.

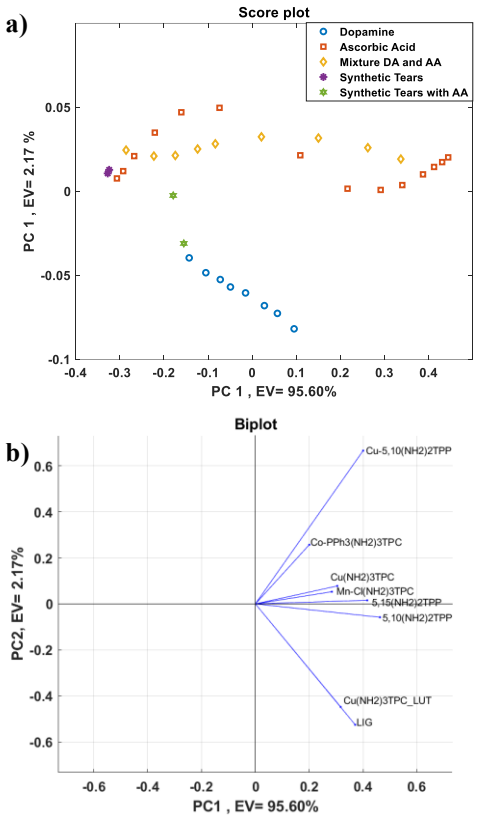

Fig 2. PCA of sensor array a) score plot based on ascorbic acid, dopamine, a mixture of dopamine and ascorbic, synthetic tears with and without ascorbic acid, b) biplot.

Reference:

[1]. Dhara, K.; Debiprosad, R.M. Review on Nanomaterials-Enabled Electrochemical Sensors for Ascorbic Acid Detection. *Anal Biochem* **2019**, *586*, 113415, doi:https://doi.org/10.1016/j.ab.2019.113415.

2. [2]. Pushparaj, K.; Catini, A.; Capuano, R.; Allegra, V.; Magna, G.; Antonelli, G.; Martinelli, E.; Agresti, A.; Pescetelli, S.; Sivalingam, Y.; et al. Nonenzymatic Potentiometric Detection of Ascorbic Acid with Porphyrin/ZnO-Functionalized Laser-Induced Graphene as an Electrode of EGFET Sensors. *ACS Omega* **2024**, *9*, 10650–10659, doi:10.1021/acsomega.3c09141.

3. [3]. Di Zazzo, L.; Kumar, A.; Meunier-Prest, R.; Di Natale, C.; Paolesse, R.; Bouvet, M. Electrosynthesized Copper Polycorroles as Versatile Materials in Double Lateral Heterojunctions. *Chemical Engineering Journal* **2023**, *458*, 141465, doi:https://doi.org/10.1016/j.cej.2023.141465.

DOI 10.5162/EUROSENSORSXXXVI/OT6.137

Insights into Graphene-Based Sensors for VOC biomarkers of lung cancer: A DFT Perspective

Ivan Shtepliuk[1], Jens Eriksson[2], Donatella Puglisi[2]
[1]Semiconductor Materials Division, Department of Physics, Chemistry and Biology-IFM, Linköping University, S-58183 Linköping, Sweden
[2]Sensor and Actuator Systems (SAS) Division, Department of Physics, Chemistry and Biology-IFM, Linköping University, S-58183 Linköping, Sweden

Corresponding Author's e-mail address: ivan.shtepliuk@liu.se

Summary:
In this work, we address key scientific questions regarding the use of graphene for lung cancer biomarker detection. The volatile organic compound (VOC) biomarkers of lung cancer were classified into nonpolar, polar with small dipole moments, and polar with large dipole moments. Using density functional theory (DFT) calculations, we examine the adsorption capacities of various VOC biomarkers on graphene surface. The analysis of binding energies provides valuable insights for designing sensitive and selective sensors for detecting lung cancer VOC biomarkers using graphene, potentially advancing early diagnosis and treatment of this disease.

Keywords: graphene, volatile organic compounds, lung cancer, density functional theory, adsorption.

Background and Motivation

Volatile organic compounds present in exhaled human breath and/or bioliquids e.g., blood can be considered as bioindicators of lung cancer [1]. There are at least 22 polar or non-polar VOCs [2, 3] that discriminate between healthy and lung cancer patients. Many studies have been dedicated to the detection and identification of VOCs of lung cancer by using conventional techniques, such as gas chromatography, mass spectrometry, radiography, tomography, cytology, and fluorescence bronchoscopy [4-6]. Yet, these methods encounter significant challenges: i) time-intensive breath analysis; ii) non-portable screening equipment; iii) high costs; iv) limited sensitivity to small lung cancer tumors and picomolar VOC concentrations. Recent efforts focus on finding gas-sensitive materials capable of detecting picomolar VOC concentrations linked to lung cancer. Conductive polymers, metal oxides, carbon nanotubes, gold nanoparticles, and graphene-based nanomaterials (GBM) have shown promise in developing sensing platforms [7-9]. GBM, in particular, holds great potential for commercializing affordable, rapid, and reproducible sensors for biomolecule identification. Such an enhanced potential of these materials in biosensing field is governed by the unique properties of GBM (huge carrier mobility, high electrical conductivity, high signal-to-noise ratio, large surface area of 2630 m^2/g, high electron-transfer rates, and low toxicity) [10]. These features create conditions for precise detection of foreign substances due to a large detection area, fast optical and electronic response of the system, change of the conductivity even at small concentrations of surface functional groups and bioanalytes. Indeed, different authors reported on fabrication of biosensors using oxidized graphene to detect such VOCs of lung cancer as p-xylene [11], decane [12], hexanal, heptanal, undecane [5].

Despite GBM's advantages in detecting VOCs as lung cancer indicators, previous studies lack systematic results, hindering scientists' understanding of practical graphene-family nanomaterial implementation. Challenges remain: (i) lack of a standardized database for graphene-biomarker interactions and specific interaction fingerprints, (ii) unclear physical mechanisms for sensing polar and nonpolar lung cancer biomarkers, and (iii) low sensitivity to nonpolar VOCs. The differences in adsorption abilities of graphene to polar and nonpolar lung cancer biomarkers depending on solvent effect are never discussed, and a comprehensive DFT analysis on adsorption capacity of GBM to VOC biomarkers of lung cancer has not been carried out, yet. Considering the key issues mentioned, we explore ways to address these unexplored scientific questions.

Method

Gaussian 16 package is utilized to perform all DFT calculations of VOC adsorption on gra-

phene using highly parametrized, empirical M05-2X exchange-correlation functional, with 6-31G(d) basis set. The binding energy of VOCs of lung cancer to a graphene is defined as: $E_b=E_{G+VOC}-(E_G+E_{VOC})$, where E_{G+VOC} is the total energy of the interacting graphene-VOC system, E_G is the total energy of isolated graphene, E_{VOC} is the total energy of VOC molecule.

Results

To classify and systemize the VOC biomarkers, we first calculated their dipole moments (see Fig. 1). Overall, these VOCs can be divided into three major classes: (i) nonpolar VOCs (decane, benzene, 1,4-dimethyl-benzene, cyclohexane), (ii) polar VOCs with small dipole moments (2,2,4,6,6-pentamethylheptane,2-methylheptane, undecane, methylcyclopentane, 1-methyl-2-pentylcyclopropane, 3-methyloctane, 3-methylnonane, 2,4-dimethylheptane) and (iii) polar VOCs with large dipole moments (hexanal, heptanal, 1,2,4-trimethylbenzene, 1-hexene, 1-heptene, 1-methylethenylbenzene, isoprene, styrene, trichlorofluoromethane). In addition, all these biomarkers can be classified as those that: (i) contain aromatic benzene rings (styrene, benzene, propylbenzene, 1,2,4-trimethylbenzene, 1,4-dimethyl-benzene,1-methylethenylbenzene) and (ii) do not contain hexagon carbon ring (others). These features strongly influence the interaction between VOCs and graphene-family nanomaterials. Molecules with hexagonal carbon rings align parallel to the graphene plane due to π-π stacking interaction.

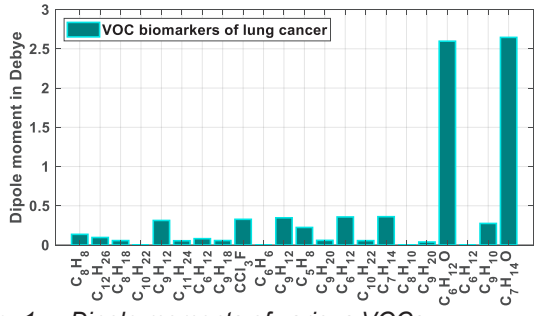

Fig. 1. Dipole moments of various VOCs.

Figure 2 shows the binding energies for each VOC on graphene. Some molecules such as 2,2,4,6,6-pentamethylheptane, undecane, and 1-methylethenylbenzene exhibit relatively high binding energies, indicating strong interactions with graphene. Aromatic compounds like styrene, propylbenzene, and benzene show moderate to high binding energies, likely due to π-π interactions with the graphene surface. VOCs with longer aliphatic chains (e.g., 2,2,4,6,6-pentamethylheptane, undecane) also show significant binding energies, possibly due to increased van der Waals interactions. The presence of functional groups (e.g., double bonds in 1-hexene, 1,4-dimethyl-benzene) may influence binding energies. The variability in binding energies suggests that a sensor based on graphene could selectively detect specific VOC biomarkers, improving the selectivity of lung cancer detection. By understanding the adsorption energies, sensor design can be optimized to target VOCs with the highest binding energies, improving sensor sensitivity.

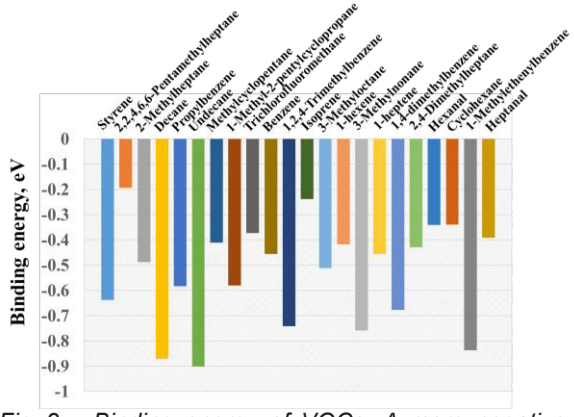

Fig. 2. Binding energy of VOCs. A more negative binding energy suggests a stronger bond to graphene.

This research was funded by the Swedish Research Council, Vetenskaprådet, grant No. 2023-07219, and Sweden's Innovation Agency, Vinnova, grant No. 2023-04186.

References

[1] S. N. Rai, et al. PLoS. ONE. 17, 11: e0277431(2022);doi:10.1371/journal.pone.0277431
[2] M. Philips, et al., *Lancet* 353, 1930 (1999); doi:10.1016/S0140-6736(98)07552-7
[3] M. Philips, R.N. Cataneo, A.J. Gagliardi, *Chest* 123, 211 (2003); doi: 10.1378/chest.123.6.2115
[4] A. Dent, et al., *Journal of Thoracic Disease*, 5, S540-S550 (2013); doi: 10.3978/j.issn.2072-1439.2013.08.44
[5] O. Barash, et al., *Lung Cancer Manage*. 2(6), 471–482 (2013); doi: 10.2217/LMT.13.58
[6] Y. Saalberg, et al., *Clinica Chimica Acta* 459, 5–9 (2016); doi: 10.1016/j.cca.2016.05.013
[7] P. J. Mazzone, *Journal of Thoracic Oncology*, 3, 774-780 (2008); doi: 10.1097/JTO.0b013e31817c7439
[8] M. P. Fernandes, et al., *Open Biomed Eng J*. 9, 228–233 (2015); doi: 10.2174/1874120701509010228
[9] Y. Li et al., *RSC Adv.* 7 (2017) 11959-11968; doi: 10.1039/c6ra25453e
[10] I. Shtepliuk, V. Khranoskyy, R. Yakimova. Semicond. *Sci. Technol.* 31, 113004 (2016); doi: 10.1088/0268-1242/31/11/113004
[11] S. Nag, et al., *J. Mater. Chem. B 2*, 6571 (2014); doi: 10.1039/C4TB01041H
[12] X. F. Zhang, et al. *Frontiers of Physics*, 11, 116801 (2016); doi: 10.1007/s11467-015-0519-4

DOI 10.5162/EUROSENSORSXXXVI/OT6.160

Microfluidic device with integrated microelectrodes for enhanced EIS sensitivity

Lilia Bató[1,2], János M. Bozorádi[1,2], Zoltán Vizvári[3], Péter Fürjes[1]

[1] Microsystems Lab., Inst. of Technical Physics and Materials Science, HUN-REN Centre for Energy Research, Budapest, Hungary
[2] Óbuda University Doctoral School on Materials Sciences and Technologies, Budapest, Hungary
[3] Symbolic Methods in Material Analysis and Tomography Research Group, Faculty of Engineering and Information Technology, University of Pecs, Pecs, Hungary

Corresponding Author: bato.lilia@ek.hun-ren.hu

Summary:
In this work a microfluidic device was created with nanostructured integrated platinum electrodes to enhance the sensitivity of Electrochemical Impedance Spectroscopy (EIS) in cell analytical applications. The sensing microelectrodes were structured using Focused Ion Beam milling creating two separate electrodes with gap sizes ranging from 200 nm to 1 µm. The decreased electrode distance allows improved sensitivity in EIS measurements, especially when a micrometer size particle or cell is trapped between the electrodes. The electrode design is supported by finite element modelling of the evolving electromagnetic field in the microfluidic channel.

Keywords: microfluidics, lab-on-a-chip, bioimpedance, electrochemical impedance spectroscopy

EIS measurements in cell analysis

In vitro study of individual cells or cell populations in a controlled chemical environment using specifically designed multifunctional microfluidic devices, such as Organ-on-Chips, offers sensitive and specific measurements that may facilitate drug discovery, screening, and the development of therapeutic strategies [1]. Combining these devices with integrated sensing systems, such as microelectrodes, can simultaneously maintain and monitor the behavior of cell populations real-time, meanwhile treating them with different chemical agents. This multidisciplinary approach can be essential in personalized medicine with further applications for antibiotic susceptibility testing [2].

Electrochemical Impedance Spectroscopy (EIS) is a non-invasive real-time technique that allows characterization of complex electrical properties of the cells while measuring the frequency dependent impedance of the system. Microelectrodes integrated inside a microfluidic system can be used for specific EIS measurements that enable cell analysis such as viability and growth monitoring. In biological applications of EIS an extensive range of frequencies is covered from 1 Hz to 10 GHz to get an insight into the inner electrochemical processes of the system regarding the electrode, the media, and the cellular properties as well. Accordingly, the spectra are divided into distinct dispersions regions α, β and γ [3]. Here, the α and β regions were measured to study both cellular and electrode properties.

Microfluidic system for EIS analysis

A compact multi-channel microfluidic system was created that can measure the EIS spectra of trapped cells using 2- or 4-electrodes architecture (Fig. 1). The central sensing microelectrodes were sectioned by Focused Ion Beam milling, creating two individual electrodes with a small gap ranging from 200 nm to 1 µm (Fig. 2). The system offers enhanced sensitivity owing to the nanometer scale electrode distances.

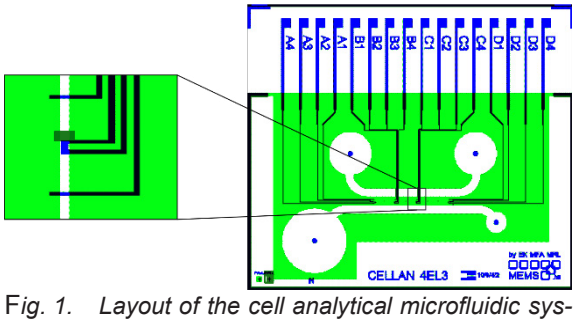

Fig. 1. Layout of the cell analytical microfluidic system and the position of the electrodes.

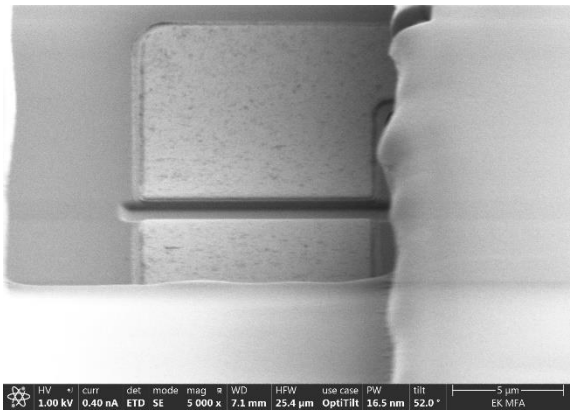

ig. 2. Sectioning the Pt electrodes with FIB milling. The gap size between the central electrodes is 1 µm.

Results

EIS measurements in 2-electrodes architecture were conducted using a PalmSens4 device, 4-electrode measurements were conducted by a bioimpedance analyzer developed by Vizvari et al. [4]. The Pt electrodes were fabricated on glass substrate, patterned by lift-off lithography. The microfluidic system contains two main inlet channels and 4 cross-channels for EIS measurements using the underlying electrodes. The cross-channels contain a trapping region, where cells or particles falling in the range of the channels' dimensions (e.g. yeast cells) can be localized over the sensing electrodes. The 10 µm deep microfluidic channels were fabricated in SU-8 by photolithography, then they were covered by a PDMS layer. The system is connected to the impedance spectroscopes via specifically designed PCBs (Fig. 3).

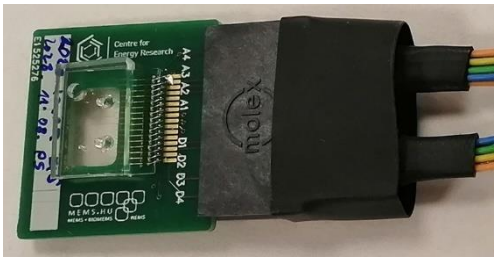

Fig. 3. The ready-to-use microfluidic device containing the cell trapping channels and the integrated electrodes.

During the measurements, the effects of the electrode distances, the stability and the reproducibility of the analytical system was characterized using different solutions, including cell culture media and cellular suspensions containing *Saccharomyces cerevisiae*. A finite element model was also developed to comprehend the electrical processes of the cellular system. The electric field developed in the channel was simulated by COMSOL Multiphysics with or without cells, the corresponding EIS spectra were compared to the corresponding measurements (Fig. 4). Initial tests with PBS, cell culture media (HEP G2) and cellular solutions yielded great reproducibility (Fig. 5). Comparison of 2- and 4-electrode measurements proved the benefit of using 4-electrodes in the low frequency range to eliminate parasitic effects.

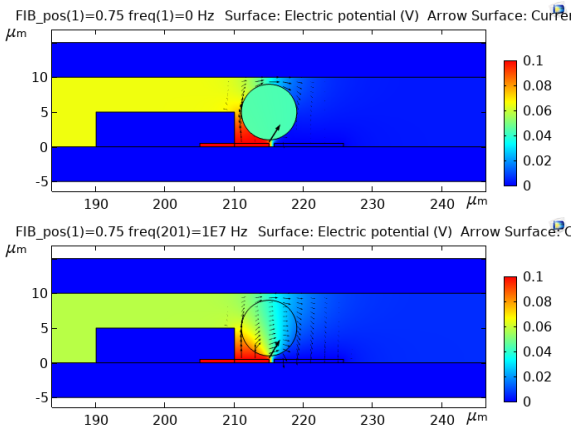

Fig. 4. FEM simulation of the electric filed over the electrodes when a cell is trapped at low (top) and high (bottom) frequencies.

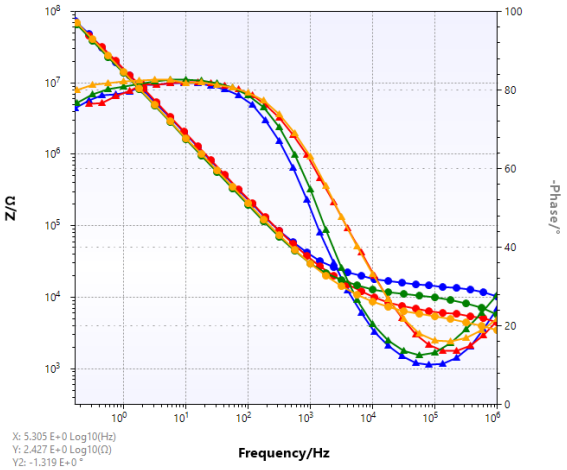

Fig. 5. Two electrode EIS spectra in PBS between two inner (red, yellow) and two outer electrodes (blue, green) in two different channels.

References

[1] L. A. Low et al., Organs-on-chips: into the next decade, *Nature Review Drug Discovery* 20, 345-361 (2020); doi: 10.1038/s41573-020-0079-3

[2] Z. Li et al., Microfluidic organ-on-a-chip system for disease modeling and drug development, *Biosensors,* 12, 370 (2022) doi: 10.3390/bios12060370

[3] K. Asami, Characterization of biological cells by dielectric spectroscopy, *Journal of Non-Crystalline Solids,* 305, 268-277 (2002) doi: 10.1016/s0022-3093(02)01110-9

[4] Z. Vizvari et al. Physical validation of a residual impedance rejection method during ultra-low frequency bio-impedance spectral measurements, *Sensors,* 20, 4686 (2020) doi: 10.3390/s201746

DOI 10.5162/EUROSENSORSXXXVI/OT6.165

Nanosensor for GHB detection in urine samples

Eva Garrido[1,2], *Antonio Valero-Martínez*[1], *Ramón Martínez-Máñez*[1,2]
[1] *Instituto Interuniversitario de Investigación de Reconocimiento Molecular y Desarrollo Tecnológico (IDM), Universitat Politècnica de València, Universitat de València, Spain,*
[2] *CIBER de Bioingeniería, Biomateriales y Nanomedicina (CIBER-BBN), 46022 Valencia, Spain*

evgarga5@upvnet.upv.es.

Summary:
In the present project, we report the design, synthesis, and evaluation of a nanosensor based on mesoporous silica nanoparticles (MSNs) loaded with a fluorescent dye and functionalized with the GABA B receptor for GHB detection in urine samples. GABA B receptor acts as a molecular gate due to its interaction with the agonist, baclofen. Subsequently, the nanodevice will be integrated into a lateral flow assay coupled with a smartphone capable of measuring the fluorescent signal produced by the released dye.

Keywords: γ-hydroxybutyric acid, chemical submission, nanosensor, human urine, lateral flow assay

Background, Motivation and Objective

γ-hydroxybutyric acid (*GHB or liquid ecstasy*), has been widely used in cases of drug-facilitated sexual assaults (DFSA) or chemical submission [1]. GHB is colorless, odorless, and soluble in aqueous media, thereby practically undetectable. On the other hand, it is quickly human metabolized and its detection in urine samples is only possible within 6-12 hours after ingestion. As a result, legislation has restricted its availability leading to GHB, consumers switching to its pro-drug, γ-butyrolactone (GBL). The precursor solvent, GBL, is used as an alternative due to its rapid conversion to GHB in the body [2]. For GHB detection, a wide variety of techniques have been used for its reliable identification in different adulterated samples, such as gas chromatography, high-performance liquid chromatography, and capillary zone electrophoresis. Likewise, some molecular probes have been used for *in situ* or *at site* GHB detection in beverages spiked but not in biological fluids such as urine.

In this scenario, gated mesoporous silica nanoparticles (MSNs) have raised considerable interest owing to the beneficial properties of the silica support such as high stability and rigidity, homogeneous and well-defined porosity (with diameters of 2–10 nm), high specific surface area and loading capacity, easily controllable morphology, and tuneable surface chemistry [3]. Although gated MSNs have been widely used in drug delivery, most prominently perhaps via pH-controlled gating, recently, the use of gated MSNs in sensing and molecular communication applications has also become more popular [4]. Sensing gated MSNs are composed of MSNs loaded for instance with selected fluorophores and functionalized with different supramolecular or biological assemblies (such as proteins [5], enzymes, antibodies, and aptamers) acting as 'molecular gates' (also known as gatekeepers or nanovalves). Gated MSNs show ideally "zero" release in the absence of an analyte, yet the presence of a target species induces, usually, a displacement of the capping ensemble, resulting in cargo delivery which is proportional to the analyte concentration. This led to a successful integration of gated MSNs materials with fluorogenic response into lateral flow assays (LFAs) with high sensitivity and selectivity for target analytes, demonstrating the tremendous potential of this approach for dipstick tests for a large range of applications. Based on the above, we report herein the design, preparation, and characterization of a nanosensor based on gated MSNs for GHB detection in urine samples (*Fig. 1*).

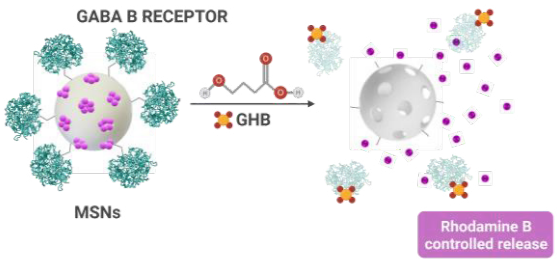

Fig. 1. Nanodevice mechanism for GHB detection in human urine.

Description of the New Method or System

To overcome the drawbacks of commercially available drug detection methods, we developed a smart nanodevice based on mesoporous silica nanoparticles (MSNs) loaded with a fluorescent dye (rhodamine B) and capped with a specific GABA B receptor which is capable of recognizing GHB in competitive media such as urine and distinguish it from the amount of endogenous GHB (*Fig. 1*). The nanosensor provides a highly useful and versatile tool for determining chemical submission drugs applicable not only in recreational environments but also potentially by law enforcement or in forensic studies. Therefore, the nanodevice is based on the interaction of GHB (produced after the hydrolysis of GBL) with the GABAergic B receptor, which will act as a molecular gate, producing the release of the encapsulated dye. In a further step, the nanodevice will be integrated into a lateral flow assay (ELF) for on-site detection of the dye-released fluorescent signal using a conventional smartphone. In this scenario, ELF assays have recently attracted attention due to their portable formats, short analysis times, low interference, low costs, and because they can be easily operated by non-specialized personnel. Additionally, ELF assays can be designed to detect multiple compounds simultaneously, providing results with high selectivity and sensitivity (ppb range), which would even allow the detection of GHB in urine samples (150 to 200 ppm).

Results

All the prepared solids were characterized by using standard techniques such as powder X-ray diffraction (PXRD), transmission electron microscopy (TEM), N_2 adsorption-desorption isotherms, elemental and thermogravimetric analyses, dynamic light scattering (DLS) and FTIR.

Once the nanoparticles were characterized, we studied rhodamine B release from MSNs (1 mg) in 800 µL of Tris-HCl buffer at pH 8.0 in the absence and presence of GBL (413 µM). The obtained payload delivery kinetics shows that in the absence of GBL, a low cargo delivery is observed, whereas in the presence of GBL, a remarkable release of rhodamine B is found. This cargo delivery agrees with GABA B receptor detachment from the surface of the nanoparticles, due to a displacement of the GABA B induced by the presence of GHB. A detection limit of roughly 80 µM was determined in aqueous solution. Encouraged by these results, we will move a step forward with the purpose of obtaining a rapid and portable test for GHB detection in urine through the integration of nanodevice into a lateral flow assay.

References

[1] L. Dufayet, S. Bargel, *et al.,* Gamma-hydroxybutyrate (GHB), 1,4-butanediol (1,4BD), and gamma-butyrolactone (GBL) intoxication: A state-of-the-art review, *Regulatory Toxicology and Pharmacology* 142, 105435-105449 (2023); doi: 10.1016/j.yrtph.2023.105435

[2] A. Procida, K. Honeychurch, Smartphone-based colorimetric determination of gamma-butyrolactone and gamma-hydroxybutyrate in alcoholic beverage samples, *Journal of Forensic Sciences* 67, 1697-1703 (2022); doi: 10.1111/1556-4029.15042

[3] A. Frickenstein, J. Hagood, *et al.,* Mesoporous Silica Nanoparticles: Properties and strategies for enhancing clinical effect, *Pharmaceutics* 13, 570-597 (2021); doi: 10.3390/pharmaceutics13040570

[4] E. Aznar, M. Oroval, *et al.,* Gated Materials for On-Command Release of Guest Molecules, *Chemical Reviews* 116, 561-718 (2016); doi: 10.1021/acs.chemrev.5b00456

[5] E. Garrido, M. Alfonso, *et al*., A Sensitive Nanosensor for the In Situ Detection of the Cannibal Drug, *ACS Sensors* 5, 2966-2972 (2020); doi: 10.1021/acssensors.0c01553

Acknowledgments

This research was supported by project PAID-06-23 funded by Universitat Politècnica de València. E. G. is grateful to the Spanish MIU and European Union-Next Regeneration EU for her “Margarita Salas” postdoctoral grant (UP2021-036).

DOI 10.5162/EUROSENSORSXXXVI/OT6.195

Aptamer-based Electrochemical Sensor for the Monitoring of Carbamazepine in Freshwater Systems

Pierrick Clément, Alba Finelli, Xavier Lefèvre, Saleem Khan, Alexandra Beard, Raphaël Pugin
Centre Suisse d'Electronique et de Microtechnique, Jaquet-Droz 1, Neuchâtel, Switzerland

pierrick.clement@csem.ch

Summary:
Carbamazepine (CBZ) is an active compound in commonly used drug and is highly durable in the environment, particularly in wastewater, which raises concerns about potential risks to animals and humans. We present an aptamer-based electrochemical sensor labelled with a redox probe which conformational change upon binding event is recorded by square-waved voltammetry. The electrochemical sensor operated in concentrations range from 2.5 pM to 250 µM in buffer. This technology provides a potential method to enable the monitoring of CBZ in treated water.

Keywords: Aptamer, electrochemical sensor, carbamazepine, environment, wastewater

Introduction

Carbamazepine (CBZ) is an anticonvulsant and anti-epileptic drug that was classified in the contaminants of emerging concern (CECs) list due to its unintended persistence in the environment notably in treated wastewater (up to 10 nM for long term exposure) [1]. Commonly used techniques to detect CBZ are liquid chromatography-tandem mass spectroscopy (LC-MS/MS), high-performance liquid chromatography (HPLC), immunoassays and solid-phase extraction (SPE) coupled with chromatography. While these methods are accurate, they are time-consuming and require sophisticated instrumentation. Furthermore, they cannot be applied for on-site detection. Several efforts have been made to develop portable assay formats using electrochemical techniques for rapid detection of carbamazepine (CBZ) and its metabolites, aiming to address this challenge. Direct electrochemical methods utilize target reduction/oxidation (redox) processes for quantification without the need for affinity reagents. While these methods are straightforward, electroactive molecules present in the medium to analyze can lead to a false positive. Molecular imprinted polymers were also reported as artificial biomimetic receptors to improve the low specificity of direct detection however, they are less selective than anti-bodies. Alternatively, aptamers are a class of short single-stranded nucleic acids that can selectively interact with their target rivalling those of antibodies. Specific sequences are generated by an in vitro molecular evolution method known as systematic evolution of ligands by exponential enrichment (SELEX). They are particularly interesting for the detection of small molecules, such as CBZ, that do not have enough immunogenicity to generate a specific antibody. In this work, we developed an electrochemical aptasensor where a conformational change is induced by CBZ target binding within the aptamer structure, which subsequently alters electron transfer between a redox tag appended at a distance and the surface of an electrode. The aptamer was modified with a thiol group on the 5′-end for immobilization on the gold sensing electrode and a methylene blue (MB) tag on the 3′-end for readout [2].

Results

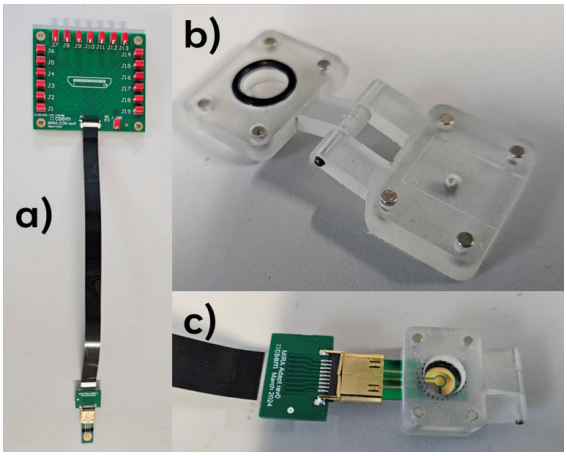

Fig 1. Picture of a) the sensing platform, b) the 3D printing cartridge and c) the sensor plugged in the HDMI mini connector with the cartridge integrated.

The gold electrodes were patterned on a silicon substrate with conventional clean room micro-

fabrication processes. Ag/AgCl electrode was deposited by aerosol jet printing technique. The chip is further integrated in an in-house developed sensing platform with a HDMI mini connector for an easy plug-and-play system. A 3D printed cartridge is integrated for drop-casting the sample on the sensor (see Fig.1). CBZ aptamer was covalently attached with the thiol function on the 3'-end by self-assembled-monolayer (SAM) on the gold working electrode overnight. For the sensor characterization, CBZ was diluted in PBS buffer (pH=7.4) at different concentrations and square-wave voltammetry (SWV) was recorded when the signal was stabilized. In Fig. 2, an increase of CBZ concentration is correlated with a decrease of the current.

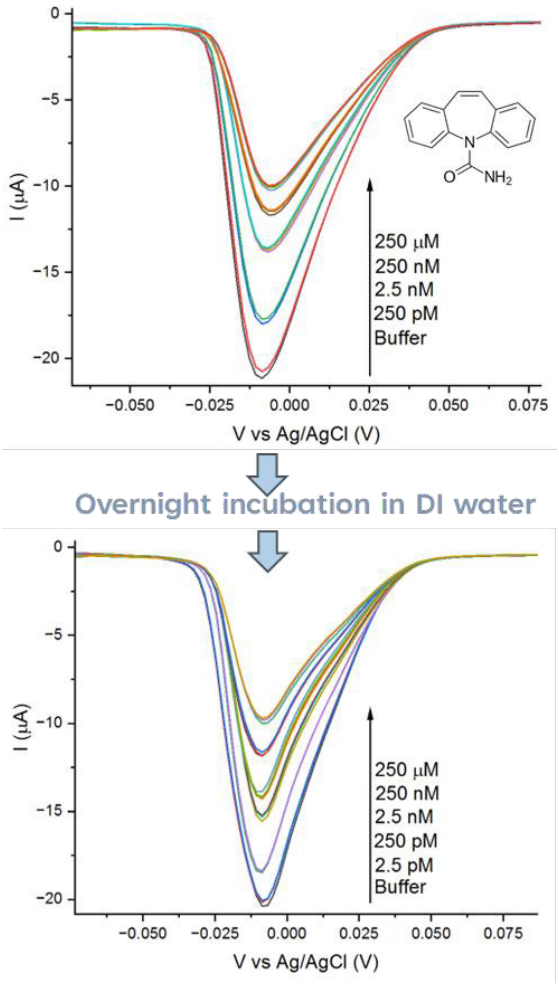

Fig. 2 SWV of the aptasensor showing its reversibility after overnight incubation in DI water.

It can be explained with the initial aptamer state being close to the gold electrode and allowing high-electron transfer rate with the MB. Upon binding with CBZ, the aptamer conformation switching moves the MB further away from the electrode which is transduced by a decrease of the current. A consequent advantage of aptamers is their reversible denaturation. By incubating the sensor in deionized (DI) water, the aptamer loses its conformation and CBZ is released in the solution. When it is reintroduced in PBS buffer, the aptamer goes back to its initial conformation and similar performances are observed as shown in Fig. 3.

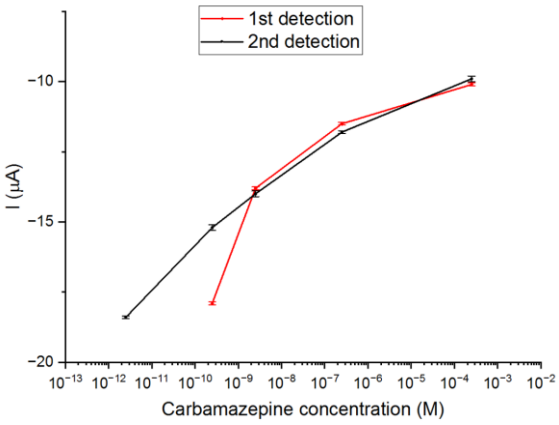

Fig. 3 Calibration curves of the aptasensor before (1st detection) and after (2nd detection) incubation in water

Conclusion

In this study, we have demonstrated the reversible detection of CBZ with a MB labelled aptamer electrochemical sensor. The developed sensor showed high sensitivity to CBZ down to 2.5 pM. Therefore, it holds great potential for the development of the next generation of portable on-site assays for the monitoring of CBZ in the environment.

References

[1] R. Fenz, A.P. Blaschke, M. Clara, H. Kroiss, D. Mascher, M. Zessner, *Water Science & Technology* 2005 52 (5), 205–213; doi: 10.2166/wst.2005.0135

[2] S. Chung, N. K. Singh, V. K. Gribkoff, D.A. Hall, *ACS Omega* 2022, 7, 39097−39106; doi: 10.1021/acsomega.2c04865

DOI 10.5162/EUROSENSORSXXXVI/OT6.196

MIP-based Sensors for Fast Nicotine Monitoring in Aerosol

Xavier Lefèvre, Pierrick Clement, Alba Finelli, Alexandra Beard, Raphaël Pugin
Centre Suisse d'Electronique et de Microtechnique, Jaquet-Droz 1, Neuchâtel, Switzerland

xavier.lefevre@csem.ch

Summary:
Nicotine is the main active component of tobacco. Its quantification in aerosols and particularly the amount delivered in lungs is of great interest to track its impact on health. Current detection methods rely on the use of mass spectroscopy coupled with liquid chromatography. However, this requires highly qualified personnel and expensive equipment. In this context, we demonstrated that Molecular Imprinted Polymers (MIP) as sensing layer deposited on electrodes are very efficient to allow fast and cheaper quantification of nicotine in aerosols.

Keywords: Molecularly imprinted polymers, nicotine detection, electrochemical sensors, fast response

Inhalation toxicological investigations and the development and pre-clinical testing of inhalable drugs require assessing the deposition kinetics of aerosol constituents on the epithelia of the respiratory tract or on in vitro models. A common in vitro approach is the deposition of the test aerosol on a trapping surface under controlled conditions, followed by quantification of deposited individual targeted aerosol constituents. This requires highly sensitive and selective analytical methodologies such as coupled chromatography - mass spectrometry, needing highly qualified personnel and expensive equipment and are not easily accessible. In this context, a promising technology for the quantification of aerosol deposition are chemically selective sensors and among them, molecularly imprinted polymers (MIP) showed very interesting abilities to selectively concentrate the target molecule for a better read-out. Matsui [1] reported one of the first nicotine MIPs in 1996. Nicotine MIPs were firstly used to preconcentrate nicotine before chromatography analysis [2] but quickly, attention turned on the analysis of cigarette smokes [3]. They also had interest for the delivery of nicotine through patches. Sensors were also developed for the analysis of residues in urines [4]. Finally, regarding detection methods, besides QCM [5], capacitive measurement [6] and optical detection [7] were used. No MIP for electrochemical detection of nicotine was mentioned. In this work, MIP were combined with electrochemical chips to build the nicotine sensors. Two approaches were evaluated: UV-curing of MIP on the electrode and electrodeposition.

MIP-based sensors are usually built by depositing preformed nanoparticles of MIP, but this leads to rather thick layers. We therefore focused on a polymer-based MIP formulation deposited as a thin film on the electrode and cured by UV exposure. The formulation is based on divinylbenzene and methacrylic acid, dicumyl peroxide being the activator of polymerization. Despite the polymer layer is insulating, we managed to deposit a very thin film (few 10ths of nanometers) to ensure sufficient recorded signal by using Pico-Pulse Jetting.

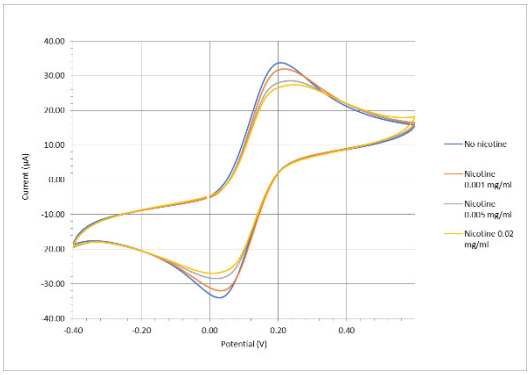

Fig. 1: detection of nicotine by MIP deposited by Pico-Pulse Jetting on working electrode of screen-printed carbon electrodes with Ag/AgCl reference.

MIP-based nicotine sensors were thus printed and further characterized. Direct monitoring of nicotine at its rather high redox potential was found to damage the sensing layer. Therefore, an indirect electrochemical measurement was developed using Fe(II)/Fe(III) as probe, avoiding high potential and deterioration of the MIP layer. This Fe(II)/Fe(III) potential value is directly linked to the presence of Nicotine and Fig. 1 shows an example of nicotine detection with this approach.

For such kind of sensors, calibration is then needed, and Fig. 2 shows a calibration curve obtained with our sensor over the nicotine concentration range of interest.

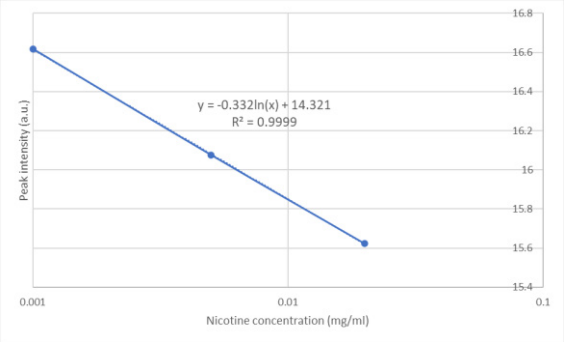

Fig. 2: calibration of MIP-based nicotine sensors fabricated by Pico-Pulse Jetting

Finally, we also investigated its sensitivity, its selectivity, and its stability. Very low amounts of nicotine (down to few ng/ml) were detectable in short times (10-15 min) allowing straightforward and fast measurements. The selectivity was very high even in presence of nicotine metabolites such as cotinine (Fig. 3). The sensor was exposed to various pH, solvents and biological media conditions and showed sufficient reliability for the foreseen application.

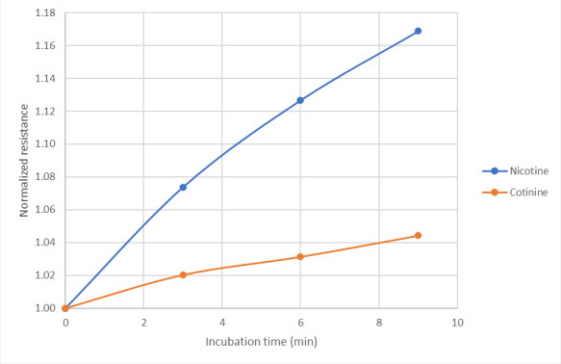

Fig. 3: selectivity of the MIP-based sensor fabricated by Pico-Pulse Jetting

Due to some limitations with in-situ UV-curing, we also studied MIP electrodeposition. For this purpose, we developed formulations and methods to reproducibly deposit MIP layers on electrodes by electrochemistry. Compared to standard MIP bulk-synthesis, this approach required the use of new electropolymerizable monomers such as aniline, pyrrole or thiophene. Several parameters allow a fine control on the created electrografted layer. The number of grafting cycles impacts the growth of the layer whereas the potential window used controls eventual cross-linking of the layer.
Formulations were then refined to increase the sensitivity and the selectivity by incorporating co-monomers such as acrylic acid or methyl acrylate. Those functional monomers promote more specific interactions with the target molecule nicotine which, in theory, enhances the selectivity. We were thus able to reach a very high sensitivity (in nanomolar/ppb range) together with keeping short analysis times (typically 3 to 5 minutes) and high selectivity.

We thus developed nicotine electrochemical sensors allowing fast and precise determination of nicotine in solution. Performances and robustness were optimized to achieve on-line measurement of nicotine levels in aerosols.

[1] J. Matsui, A. Kaneko, Y. Miyoshi, K. Yokoyama, E. Tamiya, and T. Takeuchi, “A Molecularly Imprinted Nicotine-Selective Polymer,” *Anal. Lett.*, vol. 29, no. 12, pp. 2071–2078, Sep. 1996, doi: 10.1080/00032719608002231.

[2] S. H. Hashemi and F. Keykha, “Application of the response surface methodology in the optimization of modified molecularly imprinted polymer based pipette-tip micro-solid phase extraction for spectrophotometric determination of nicotine in seawater and human plasma,” *Anal. Methods*, vol. 11, no. 42, pp. 5405–5412, 2019, doi: 10.1039/C9AY01496A.

[3] Y. Liu, S. Antwi-Boampong, J. J. BelBruno, M. A. Crane, and S. E. Tanski, “Detection of secondhand cigarette smoke via nicotine using conductive polymer films,” *Nicotine Tob. Res.*, vol. 15, no. 9, pp. 1511–1518, Sep. 2013, doi: 10.1093/ntr/ntt007.

[4] Y. Tan, J. Yin, C. Liang, H. Peng, L. Nie, and S. Yao, “A study of a new TSM bio-mimetic sensor using a molecularly imprinted polymer coating and its application for the determination of nicotine in human serum and urine,” *Bioelectrochemistry*, vol. 53, no. 2, pp. 141–148, 2001, doi: https://doi.org/10.1016/S0302-4598(00)00095-7.

[5] J. Alenus *et al.*, “Molecularly imprinted polymers as synthetic receptors for the QCM-D-based detection of l-nicotine in diluted saliva and urine samples,” *Anal. Bioanal. Chem.*, vol. 405, no. 20, pp. 6479–6487, 2013, doi: 10.1007/s00216-013-7080-1.

[6] K. Liu, W.-Z. Wei, J.-X. Zeng, X.-Y. Liu, and Y.-P. Gao, “Application of a novel electrosynthesized polydopamine-imprinted film to the capacitive sensing of nicotine,” *Anal. Bioanal. Chem.*, vol. 385, no. 4, pp. 724–729, 2006, doi: 10.1007/s00216-006-0489-z.

[7] N. Cennamo *et al.*, “A molecularly imprinted polymer on a plasmonic plastic optical fiber to detect perfluorinated compounds in water,” *Sensors*, vol. 18, no. 6, pp. 1–11, 2018, doi: 10.3390/s18061836.

DOI 10.5162/EUROSENSORSXXXVI/OT6.214

Micromachined SU-8/PMMA Sandwich Electrodes with Functional Graphene Coatings for Biopotential Monitoring

Seba Nur Alhasan[1], S. Sajjad Mirbakht[1], Saygun Guler[1], Osman Sahin[1], Muhammad Umar[1], Burcu Arman Kuzubasoglu[1], Murat Kaya Yapici[1,2,3]

[1] Faculty of Engineering and Natural Sciences, Sabanci University, Istanbul 34956, Turkey

[2] Department of Electrical Engineering, University of Washington, Seattle, WA 98195, USA

[3] Sabanci University Nanotechnology Research and Application Center, Istanbul 34956, Turkey

Corresponding author: murat.yapici@sabanciuniv.edu

Summary:

Dry electrodes with high human biopotential signal recording quality is the promising future for wearable long-term health monitoring devices. Here, we present an ultrathin and flexible textile-like electrode composed of double-layered SU-8/PMMA microstructure fabricated using lithography-based microfabrication techniques featuring structures as fine as 100μm. Graphene oxide (GO) is introduced to the electrodes as an electrically conductive material using a single-step dip-coating method. To improve the electrical conductivity of the coated GO and hence, the performance of the electrodes, a reduction step using eco-friendly vitamin C (L-ascorbic acid) was carried out to transform GO to reduced graphene oxide (rGO). Our experimentation involved recording lead-I ECG signal acquisition using the fabricated electrodes, demonstrating their superior performance compared with Ag/AgCl wet electrodes with similarity up to 98.84% with distinguishable QRS peaks. The results pave the way towards a clinical-grade ECG signal performance.

Keywords: dry electrode, ECG, graphene oxide, microfabrication, vitamin C.

Introduction

Cardiovascular monitoring using electrocardiography (ECG) is an established technique to monitor the activity of the heart [1]. Typically Ag/AgCl wet electrodes are used to acquire biopotential signals such ECG [2]. Although these wet electrodes show highly accurate performance, they have various issues like the conductive gels drying out over time and problems with skin irritation [3]. In this study we propose a novel fabrication flow with the use of a hard mask (protection layer) avoiding the use of electron beam lithography (EBL). This work utilized industrial acrylic-based PMMA and SU-8; an epoxy-based material, to create textile-like mesh. The mesh arrangement of textile weaves makes these electrodes suitable for biopotential measurements on the skin, as this structure inherently guides signal energy in the "*z*" direction, perpendicular to the skin surface. To functionalize the electrode, graphene oxide was utilized, taking advantage of the superior capabilities of a simple, eco-friendly green reduction method using L-ascorbic acid.

Electrode fabrication

The fabrication (Fig. 1a) starts with depositing a 200 nm of SiO2 as sacrificial layer. Then as supportive material 50 um negative photoresists SU-8-50 was spin coated at 3000 rpm then soft-baked at 65 °C for 7 min and 95 °C for 20 min then exposed to a dose of 140 mJ ultraviolet (UV) to produce a square-type microarray, post-exposure bake was then performed at 65 °C for 1 min and 95 °C for 6 min. The sample was then immersed in SU-8 developer. The next layer was PMMA, 495K MW PMMA-C4 was spin coated at 4000 rpm and was baked at 180° C for 10 min to produce 300nm. To selectively etch the PMMA, a layer of copper (Cu) was deposited on top of it.The copper layer was then patterned by spin-coating AZ5214 photoresist (PR) and exposed to UV light. Then O_2 plasma was performed for 3 minutes to etch the exposed regions of PMMA. After patterning the PMMA the Cu layer was removed by an etchant mixture of acetic acid and hydrogen solution. Finally, the electrode was released by immersion inside buffered oxide etch BOE 7:1 for 5 h. The released SU-8/PMMA sample was drop-casted by diluted GO graphene oxide suspension (4mg/mL) on a hydrophobic Teflon surface to confirm a uniform coating and dried at room temperature for one day. Next, the sample was immersed in 0.5 g/ml L-ascorbic acid and deionized water for three days at room tempera-

ture. After the reduction, the sample was washed by deionized water and left to dry (Fig. 1b). The electrode internal layers after wiring are demonstrated in Fig. 1c.

ECG signal recording

Data acquisition utilized an open-source unit (Cyton Board, OpenBCI) and recorded signals were processed using MATLAB. Electrocardiogram signals were recorded and compared with microfabricated electrodes against clinical-grade wet Ag/AgCl electrodes in a single-lead setup. The placement and an image of the microfabricated electrode during signal acquisition were illustrated in Fig. 1d.

Results and Conclusion

The resistance of the textile-like electrode was measured by a desktop multimeter and showed a relatively low resistance of 0.5 kΩ upon reduction. The flexibility of the electrodes was demonstrated in Fig. 1e, and their microscope images with and without rGO. The correlation function between the signals over a 10-second period was calculated to be 98.84%, indicating a strong correlation. This high correlation serves as validation for the high performance of the TPM electrode in capturing biopotential signals. Fig. 1f displays the two signals recorded over 10-second intervals.

Acknowledgments

Professor Murat Kaya Yapici appreciates the support of the Turkish Academy of Sciences (TUBA GEBIP'21) and the Science Academy (BAGEP'23).

References

[1] S. Savonitto et al., Prognostic value of the admission electrocardiogram in acute coronary syndromes, JAMA 281, (1999); doi: 10.1001/jama.281.8.707

[2] M. K. Yapici et al., Graphene-clad textile electrodes for electrocardiogram monitoring, Sens Actuators B 221, (2015); doi: 10.1016/j.snb.2015.07.111

[3] L. McNichol et al., Medical adhesives and patient safety: State of the science consensus statements for the assessment, prevention, and treatment of adhesive-related skin injuries, J. Wound, Ostomy Continence Nursing, 40, (2013); doi: 10.1097/WON.0b013e3182995516

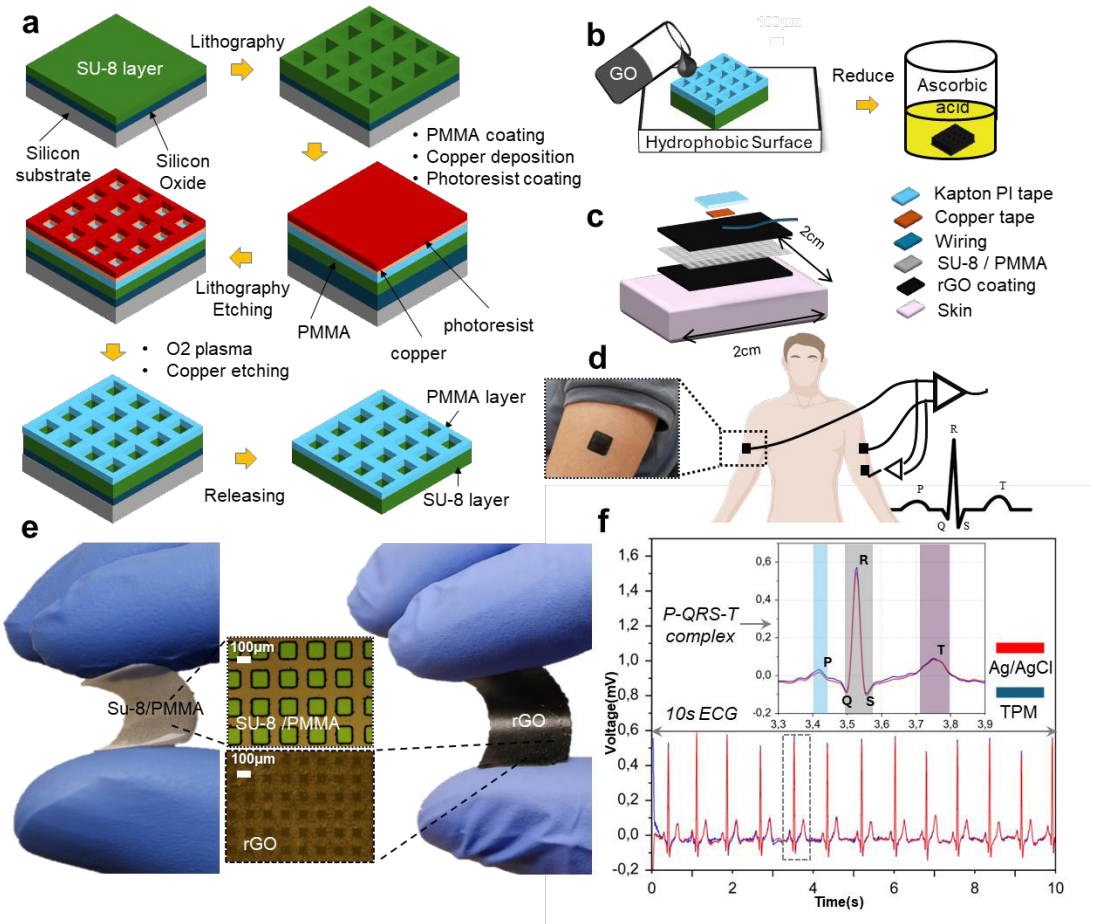

Fig. 1. (a) Fabrication steps of TPM electrode, (b) GO coating-reduction process, (c) exploded view of a TPM electrode showing its inner layers, (d) images of the electrode placed on the upper arm, (e) flexibility test applied by manually bending the electrode with under microscope images, and (f) Simultaneous ECG recording with textile-like electrodes and Ag/AgCl electrode

DOI 10.5162/EUROSENSORSXXXVI/OT6.217

3D Modelling of droplet formation in two-phase microfluidics for single-cell manipulation

Zsombor Szomor[1,2], *Eszter L. Tóth*[1], *Péter Fürjes*[1]

[1] *Microsystems Lab., Inst. of Technical Physics and Materials Science, HUN-REN Centre for Energy Research, Budapest, Hungary*
[2] *Óbuda University Doctoral School on Materials Sciences and Technologies, Budapest, Hungary*

Corresponding Author: szomor.zsombor@ek.hun-ren.hu

Summary:
In this study, the evolving hydrodynamic phenomena were modelled and characterized in complex two-phase micro-fluidic systems, aiming to enhance their applicability in advanced droplet-based single-cell sorting and analytical methodologies. An innovative Computational Fluid Dynamics (CFD) driven multi-dimensional optimization strategy was introduced and applied to explore the influence of geometric configurations and flow parameters. The droplet generation process has been studied by finite element modelling (FEM), utilizing the Laminar Flow and Level Set modules within COMSOL Multiphysics for numerical simulations. The proposed microfluidic system was manufactured and its behaviour was compared to the simulated characteristics. The experimental results supported the comprehension of the droplet formation in case variable volumetric flow rates and the interaction between flow dynamics and channel geometry. The effective control of the resultant droplet size distribution enables to determine the numbers of particles and cells confined.

Keywords: finite element modelling (FEM), two-phase microfluidics, single-cell, droplet formation, LoC

Motivation and Objectives

In the past twenty years, the adoption of micro-engineered systems has transformed the high-throughput analysis methods applied in the fields of chemical and biological sciences. Droplet-based microfluidic systems generate and manipulate distinct, physically separated fluid volumes or droplets. These multi-phase flow systems enable to utilise a wide range of easily accessible techniques for manipulating droplets, including splitting, merging, mixing, dilution and incubation. Droplets produced within two-phase microfluidic setups serve as optimal vessels for high-throughput cell screening applications. The response of individual cells to physical and chemical effects can be precisely examined in the micro-environment at the scale of cell size. This study employs high-performance finite element modelling (FEM) of these multi-phase systems for a thorough examination of hydrodynamic droplet generation process, primarily focusing on the effects of different flow rates and geometric parameters [1].

Fluid Dynamic Simulation Methods

COMSOL Multiphysics simulation code was employed to examine the droplet formation process in 3D two-phase models, aiming for a more precise understanding of the evolving flow characteristics. The analysis relies on numerically solving the governing Navier-Stokes and continuity equations. To characterize and compare microfluidic systems, the Capillary number (Ca) served as a commonly utilized parameter. Regarding droplet generation, including evolving droplet diameters and generation frequencies, the effects of volume flow ratios at the inlets, fluid viscosity, and interface tension were explored through successive parametric sweep simulations. Details of the main material properties of the fluids are provided in Table 1.

Tab. 1: Main material parameters of fluids

Material	Dynamic viscosity (μ)	Density (ρ)
Water	$1.95 \cdot 10^{-3}$ *Pa·s*	10^3 *kg/m³*
Silicon Oil	$20 \cdot 10^{-3}$ *Pa·s*	10^3 *kg/m³*

To manage reliable simulation of multiphase fluid flow, the Level Set technique, a robust computational approach was employed [2, 3]. This method was integrated with the Laminar Flow module to obtain precise results within the microfluidic approaches characterized by a predomi-

nance of low Reynolds numbers. The droplet diameters were calculated using a self-developed MATLAB script, which based on image analysis.

Numerical Results

According to the simulations, a significant change can be detected in the droplet diameters as the function of the flow rate and different geometric properties (Fig. 1). The average diameter was decreased from 98.27 µm to 62.16 µm when the flow rate of oil increased from 1.2 µl/s to 3.2 µl/s. The flow rate of water remained constant (0.2 µl/s). The size distribution of generated droplets was visualised by histograms created using the MATLAB software (Fig. 2).

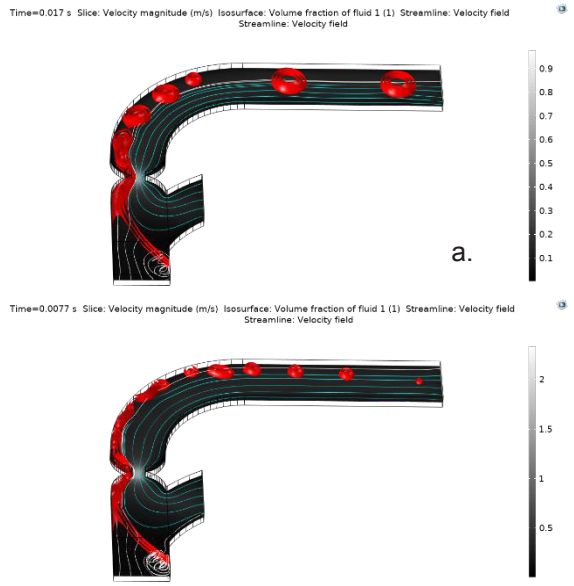

Fig. 1. Droplet generation in the 3D FEM model in the case of two different flow rates. The applied flow rates were: 0.2 µl/s (water), 1.2 µl/s (oil) in Figure 1.a and 0.2 µl/s (water), 3.2 µl/s (oil) in Figure 1.b.

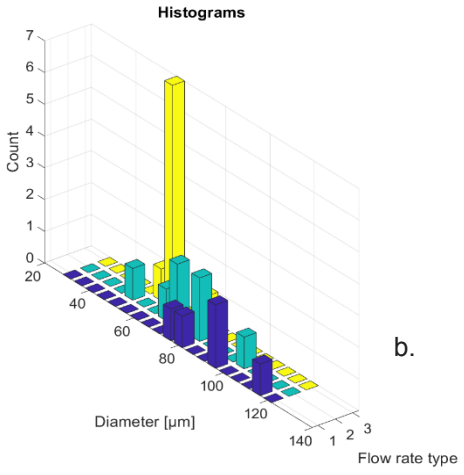

Fig. 2. Droplet size distributions based on the image analysis of the simulated droplet generation. While the flow rate of water was set to a constant value of 0.2 µl/s, three different oil flow rates were varied between 1.2 µl/s (1), 2 µl/s (2), and 3.2 µl/s (3).

Experimental Validation

To validate the numerical model, microfluidic devices were manufactured using soft lithography techniques in Polydimethylsiloxane (PDMS) polymer, featuring various geometrical configurations for droplet generation (Fig. 3). Experimental results indicate that factors such as the wetting characteristics of the aqueous phase significantly affect the frequency of droplet formation, whereas the velocity of the oil phase impacts the droplet size. Elevating either the flow rate of the oil phase or the Capillary number leads to a momentous reduction in droplet diameter.

The obtained results can support the establishment and optimisation of multi-phase microfluidic systems to achieve proposed size of microdroplets applicable as miniaturized reactors or cell containers in Lab-on-a-Chip and Organ-on-chip applications.

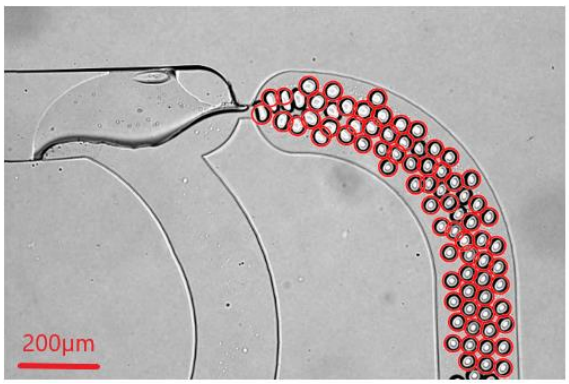

Fig. 3. Laboratory experiment to support the validation simulation results. The flow rate was set as 0.1 µl/s (water), 0.2 µl/s (oil). The droplet diameters were determined by MATLAB. The average diameter was 44.57 µm in this case.

References

[1] K. J. Donovan. „Computational fluid dynamics modeling of two - dimensional and three – dimesional segmented flow in microfluidic chips”, San Jose State University, (2014). doi:10.31979/etd.3tzd-y6xm.

[2] H. A. Akhlaghi Amiri, A. A. Hamouda, „Evaluation of level set and phase field methods in modeling two phase flow with viscosity contrast through dual-permeability porous medium”, Elsevier, International Journal of Multiphase Flow, (2013)

[3] „Two Methods for Modeling Free Surfaces in COMSOL Multiphysics”, url: https://www.comsol.com/blogs/two-methods-for-modeling-free-surfaces-in-comsol-multiphysics/ (last access: 04-24-2024)

DOI 10.5162/EUROSENSORSXXXVI/OT6.228

A Simple Microfluidic System for Point-of-Care Therapeutic Drug Monitoring of Anticancer Drugs

András Füredi[1,2], Dóra Bereczki[1,3], Balázs Gombos[2,4], Pál Szabó[5], Péter Vajdovich[6], Péter Fürjes[1]

[1] Microsystems Lab., Inst. of Technical Physics and Materials Science, HUN-REN Centre for Energy Research, Budapest, Hungary,
[2] Drug Resistance Research Group, Institute of Molecular Life Sciences, HUN-REN Research Centre for Natural Sciences, Budapest, Hungary
[3] Óbuda University Doctoral School on Materials Sciences and Technologies, Budapest, Hungary
[4] Semmelweis University Doctoral School, Budapest, Hungary
[5] Centre for Structural Science, HUN-REN Research Centre for Natural Sciences, Budapest, Hungary
[6] Department of Clinical Pathology and Oncology, University of Veterinary Medicine Budapest, Budapest, Hungary

Corresponding Author: furedi.andras@ek.hun-ren.hu

Summary:

Therapeutic Drug Monitoring (TDM) would be a game changer for cancer therapy, however due to the current methods applied to follow the drug concentrations in the blood are expensive and require specialized expertise and instruments. Point-of-Care (PoC) TDM system has never realized. Here we present a fluorescence-based PoC microfluidic solution to monitor blood levels of anticancer agents. Using blood samples from mouse models of malignancies and veterinary cancer patients we prove our approach to be suitable for TDM in an experimental environment and have the potential to ultimately personalize chemotherapy.

Keywords: chemotherapy, therapeutic drug monitoring, drug resistance, microfluidics, fluorescence

Background, Motivation an Objective

Cancer claims almost 10 million lives annually, making it one of the major causes of death. Chemotherapy (CT) is a widely used option to treat malignancies, however CT protocols are established on a “one size fits all” basis and ignore inter-patient differences in drug pharmacokinetics which influence the blood levels of anticancer drugs, therefore leading to improper dosing in 50% of patients [1]. Missing target blood concentration will lead to drug resistance and/or unwanted side effects. Therapeutic Drug Monitoring (TDM) could be the key to improve and personalize CT, however the lack of an affordable Point-of-Care method is preventing its introduction to oncology. Mass spectrometry (MS) is the golden standard analytical approach to determine blood drug levels, but the instrument and specialized expertise to operate it are rarely available in the clinical environment. The high volume of blood required for MS analysis is also a challenge, because cancer patients are regularly weakened.

A Novel Microfluidic TDM Method

Exploiting the strong and specific fluorescence of anthracyclines [2], the most used CT agents, we propose a radically new microfluidic chip-based approach to rapidly determine plasma concentrations of several widely applied anticancer drugs (Figure 1.). Microvolume plasma separation and collection from a drop of blood (>50 μl) will be done with a specifically designed microfluidic chip, then plasma anthracycline concentration will be measured using a compatible spectrophotometer.

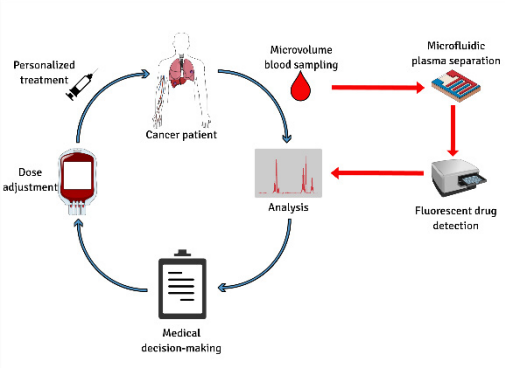

Fig 1. Our novel concept for microfluidic TDM.

Results

Anthracyclines (doxorubicin, daunorubicin, epirubicin, idarubicin, mitoxantrone, pixantrone) are not only the most effective anticancer chemotherapeutics, but they are also highly fluorescent. First, we showed that after sample preparation this autofluorescence is enough to detect doxorubicin (DOX, excitation: 490 nm, emission: 590 nm) in different solvents in a concentration dependent manner using 100 µl sample in a Tecan Spark fluorescent plate reader. To further reduce the required volume of sample, we designed a simple microfluidic chip with autonomous sample transport and proved the significant sample volume reduction (to ~ 7 µl) had no significant effect on the efficiency of fluorescence detection. The sensitivity and precision of the fluorescent measurements were validated by mass spectrometry based (Sciex 5600+ QTof) concentration determination. For the in vivo evaluation of our approach, we treated a mouse model of triple negative breast cancer with 6 mg/kg of pegylated liposomal doxorubicin (PLD) intravenously and took blood samples at 5 time points through retro-orbital bleeding. As Figure 2. shows, the individual pharmacokinetics of a mouse was determined, and the results were highly similar to the mass spectrometry measurements.

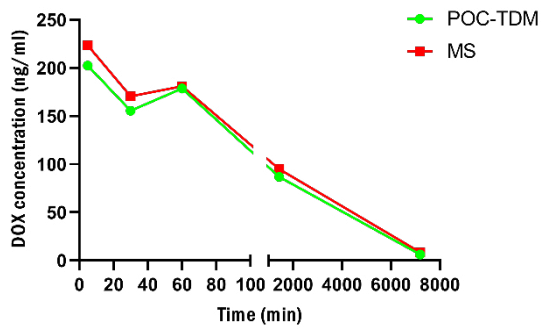

Fig 2. A representative pharmacokinetics curve of a single mouse treated with 6 mg/kg PLD. Blood concentrations measured by our point-of-care TDM chip (POC-TDM, green) was also determined by mass spectrometry (MS, red).

Furthermore, we tested our method in the veterinary clinical setting by analyzing blood samples from a cat cancer patient diagnosed with feline injection-site sarcoma (FISS). First, the patient was treated with epirubicin (25 mg/m^2, constant rate infusion for 60 minutes), but after there was no tumor response and the disease further progressed, the therapy was changed to PLD (1 mg/kg, constant rate infusion for 60 minutes) which stabilized the tumor and reduced its size. Comparing the pharmacokinetics of epirubicin and PLD revealed that, while epirubicin levels dropped significantly 60 minutes after administration, DOX concentrations was approximately 10 times higher, and it was not changed significantly in 270 minutes (Fig 3.).

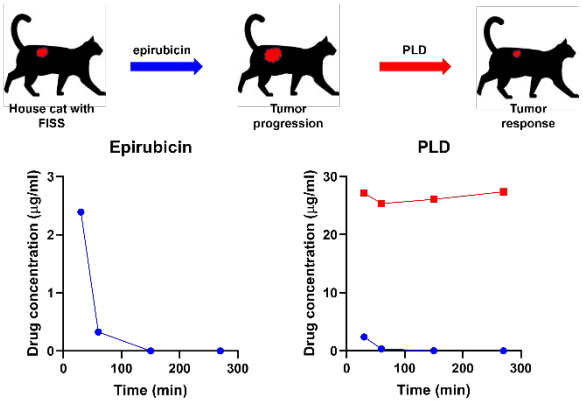

Fig 3. Our TDM method is capable of measuring epirubicin and DOX levels in veterinary patients. The progression of the FISS tumor was not influenced by epirubicin (blue) treatment, but PLD (red) therapy was partially successful due to the higher blood concentrations and longer circulation time.

PLD's increased concentration and retention time over epirubicin was a result of the liposomal formulation which shields DOX from enzymatic inactivation and metabolism [3].

Conclusion

As new anthracycline-based combinational therapies proved to be surprisingly efficient in various cancers [4], the need for more patient-tailored dosing is rising. We have established a novel POC-TDM microfluidic chip and a method to measure personal pharmacokinetics of individual patients treated with anthracycline chemotherapies ultimately opening a new avenue to personalized cancer care.

References

[1] J. Rebollo, B. Valenzuela, Use of therapeutic drug monitoring of cancer chemotherapy to modify initial per-protocol doses, Journal of Clinical Oncology, e13015 (2010), doi: 10.1200/jco.2010.28.15_suppl.e13015.

[2] N.S. Motlagh, P. Parvin, Fluorescence properties of several chemotherapy drugs: doxorubicin, paclitaxel and bleomycin, Biomedical Optics Express, (2016), doi: 10.1364/BOE.7.002400.

[3] A. Füredi, K. Szebényi, Pegylated liposomal formulation of doxorubicin overcomes drug resistance in a genetically engineered mouse model of breast cancer, Journal of Controlled Release, (2017), doi: 10.1016/j.jconrel.2017.07.010.

[4] K. Szebényi, A. Füredi, Effective targeting of breast cancer by the inhibition of P-glycoprotein mediated removal of toxic lipid peroxidation by-products from drug tolerant persister cells, Drug Resistance Updates, (2023), doi: 10.1016/j.drup.2023.101007